Basin Research (2009) **21**, 91–109, doi: 10.1111/j.1365-2117.2008.00372.x

Plio-Quaternary sediment budget between thrust belt erosion and foreland deposition in the central Andes, southern Bolivia

J. B. Barnes*,† and W. A. Heins*

*ExxonMobil Upstream Research Co., Houston, TX, USA

†Department of Geological Sciences, University of Michigan, Ann Arbor, MI, USA

ABSTRACT

Estimates of the physical boundary conditions on sediment source and sink regions and the flux between them provide insights into the evolution of topography and associated sedimentary basins. We present a regional-scale, Plio-Quaternary to recent sediment budget analysis of the Grande, Parapeti and Pilcomayo drainages of the central Andean fold-thrust belt and related deposits in the Chaco foreland of southern Bolivia (18–23°S). We constrain source-sink dimensions, fluxes and their errors with topographic maps, satellite imagery, a hydrologically conditioned digital elevation model, reconstructions of the San Juan del Oro (SJDO) erosion surface, foreland sediment isopachs and estimated denudation rates. Modern drainages range from 7453 to 86 798 km^2 for a total source area of 153 632 km^2. Palaeo-drainage areas range from 9336 to 52 620 km^2 and total 100 706 km^2, suggesting basin source area growth of $\sim$50% since $\sim$10 Ma. About 2.4–3.1 $\times$ 10^4 km^3 were excavated from below the SJDO surface since $\sim$3 Ma. The modern foredeep is 132 080 km^2 with fluvial megafan areas and volumes ranging from 6142 to 22 511 km^2 and from 1511 to 3332 km^3, respectively. Since Emborozú Formation deposition beginning 2.1 $\pm$ 0.2 Ma, the foreland has a fill of $\sim$6.4 $\times$ 10^4 km^3. The volume and rate of deposition require that at least $\sim$40–60% of additional sediment be supplied beyond that incised from below the SJDO. The data also place a lower limit of $\geq$ 0.2 mm year^{-1} (perhaps $\geq$ 0.4 mm year^{-1}) on the time- and space-averaged source area denudation rate since $\sim$2–3 Ma. These rates are within the median range measured for the Neogene, but are up to 2 orders of magnitude higher than some observations, as well as analytic solutions for basin topography and stratigraphy using a two-dimensional mathematical model of foreland basin evolution. Source-to-sink sediment budget analyses and associated interpretations must explicitly and quantitatively reconcile all available area, volume and rate observations because of their inherent imprecision and the potential for magnification when they are convolved.

INTRODUCTION

The sediment-routing system links sources to sinks, determining how mountains erode, how topography evolves, and how landscapes translate into the sedimentary record (Allen, 2008). Sediment sources and sinks are coupled through various surface processes and their fluxes to the extent that mountain belt deformation can be influenced by deposition downstream (e.g. Flemings & Jordan, 1989; Beaumont *et al.*, 2000; Simpson, 2006). Unfortunately, questions remain about what combination of factors influence the volume and rate of sediment production, the spatial variability of sediment production within the source, and the rate of sediment delivery to the sink (Tucker & Slingerland, 1996; Stock *et al.*, 2006; Phillips & Gomez, 2007). Sediment delivery rates are a particularly important control on the dimensions and physical characteristics of basin-filling sediments (Hovius & Leeder, 1998). If estimates of the volume and mass flux (among other things) from the source area are available, then quantitative tools can be used to predict sedimentary architecture (Robinson & Slingerland, 1998a, b; Geslin *et al.*, 2001, 2002; Clevis, 2003; Clevis *et al.*, 2003; Van Wagoner *et al.*, 2003; Overeem *et al.*, 2005; Robin *et al.*, 2005) and reservoir quality (Lander & Walderhaug, 1999; Perez *et al.*, 1999; Bray *et al.*, 2000; Bonnell & Lander, 2003) in sedimentary basins.

A mass balance approach has been used to quantify sediment budgets for the Alps, Appalachians, Himalayas and Rocky Mountains by integrating river sediment loads, palaeogeographic reconstructions, seismic data and the stratigraphic record (Hay *et al.*, 1992; Le Pichon *et al.*, 1992; Curray, 1994; Einsele *et al.*, 1996; Pazzaglia & Brandon, 1996; Kuhlemann *et al.*, 2001, 2002; Schlunegger *et al.*, 2001; Clift *et al.*, 2002; Clift, 2006; McMillan *et al.*, 2006). These

Correspondence: Jason Barnes, Department of Geological Sciences, University of Michigan, 1100 N. University, Ann Arbor, MI48109–1005, USA. E-mail: barnesja@umich.edu.

sediment budgets provide some of the best constraints for inferring mountain palaeotopography and estimating denudation rates, but uncertainties are often large and/or not quantified because of the scales over which they are applied.

Active fold-thrust belts and their foreland basin systems are sources and sinks closely linked in space and time that possess a variety of evidence that can be used to constrain their sediment budget (Fig. 1) (DeCelles & Giles, 1996; Critelli, 1999; Critelli *et al*., 2003). For example, many thrust belts have palaeosurfaces, formed by periods of protracted erosion (Widdowson, 1997), that have been used as markers to (a) estimate uplift magnitudes (de Sitter, 1952; Epis & Chapin, 1975; Scott, 1975; Kennan, 2000; Barke & Lamb, 2006), (b) estimate exhumation magnitudes (Sobel & Strecker, 2003; Babault *et al*., 2005; McMillan *et al*., 2006), (c) reconstruct palaeo-drainage networks (Kennan *et al*., 1997; Kennan, 2000), (d) constrain the deformation history (Gubbels *et al*., 1993; Clark *et al*., 2006) and (e) calculate the amount of material removed from below the surface by post-formation incision (Kennan *et al*., 1997; McMillan *et al*., 2006). In the sink, flexure associated with the adjacent topographic load creates a foreland basin consisting of wedgetop, foredeep, forebulge and backbulge depozones (DeCelles & Giles, 1996). Fluvial megafans (typically 10^3–10^5 km^2, with low gradients of 0.01–0.1°) are distinguishable sediment bodies that can be dominant features of some forelands (Gohain & Parkash, 1990; Gupta, 1997; DeCelles & Cavazza, 1999; Leier *et al*., 2005). Additionally, isopach maps constructed from measured sections, geochronology, seismic data, and well logs provide constraints on the spatio-temporal distribution of the foreland-filling sediments (e.g. Uba *et al*., 2006). This foreland sedimentary record is shaped by thrust belt topography, tectonics, climate, erosion, lithology, drainage patterns and base level (Dickinson, 1974; Flemings & Jordan, 1989; Damanti, 1993; Devlin *et al*., 1993; Patterson *et al*., 1995; Van Wagoner, 1995; Burgess & Allen, 1996; Tucker & Slingerland, 1996; Schlunegger *et al*., 1997; Leeder *et al*., 1998; Geslin *et al*., 2002). Although prior studies have characterized sediment source and sink dimensions and determined erosion rates, few attempts have been made to quantify regional-scale sediment budgets and associated uncertainties in thrust belt-foreland settings.

The goal of this paper is to quantify the sediment budget for the central Andean fold-thrust belt and foreland in southern Bolivia since the Plio-Quaternary (~3–0 Ma). We account for the area, volume and rates of sediment removed from the upland sources and deposited within the downstream sink, specifically fluvial megafans and the foredeep. The following logic governs our analysis. The amount of sediment produced must fall within limits imposed by the size of the drainage, the rate and duration of denudation, and the volume of deposited sediment. The amount of sediment generated must be at least as great as the amount of sediment deposited in the proximal foredeep. The generated sediment cannot be greater than the amount denuded from the present-day drainage at the maximum estimated rate of denudation over the longest possible denudation time. This lower sediment-production limit excludes some combinations of size, rate and duration placing improved constraints on the large range of denudation rates estimated.

WHY SOUTHERN BOLIVIA?

The central Andean fold-thrust belt and Chaco foreland of southern Bolivia (18–23°S) is well suited for quantifying a Plio-Quaternary sediment budget (Fig. 2). Fluvial megafans have been important foreland depositional features since the mid-Tertiary and currently occupy most of the Chaco plain (Horton & DeCelles, 2001). Isopachs quantify the spatial and temporal distribution of the Chaco sedi-

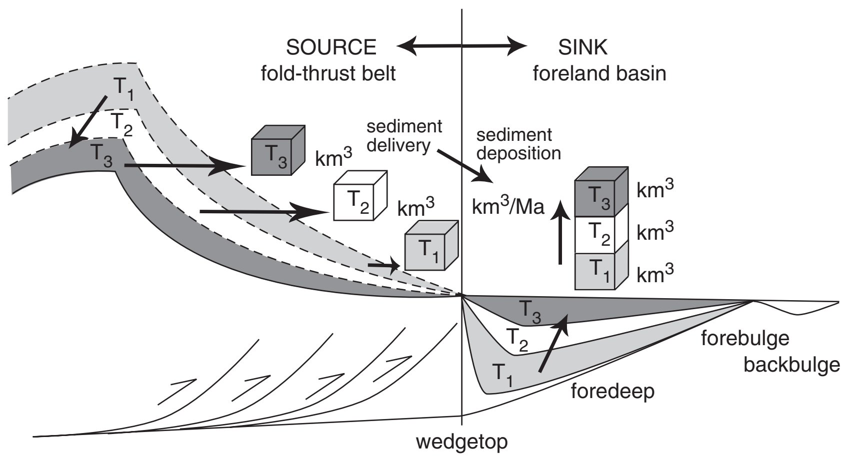

Fig. 1. Schematic thrust belt-foreland basin system sediment budget in cross-section. Eroded and deposited sediment volumes (grey to white shaded regions and boxes) for time slices T_1–T_3 (increasing to the present) from a thrust belt hinterland source to an adjacent foredeep sink, respectively. The hinterland topographic evolution from ancient (dashed) to modern (solid) time and the equivalent sink foreland sedimentary evolution are also shown. In this ideal case, boxes T_1–T_3 in the source are the same size as the equivalent boxes in the sink. For simplicity, no thrust belt propagation is shown.

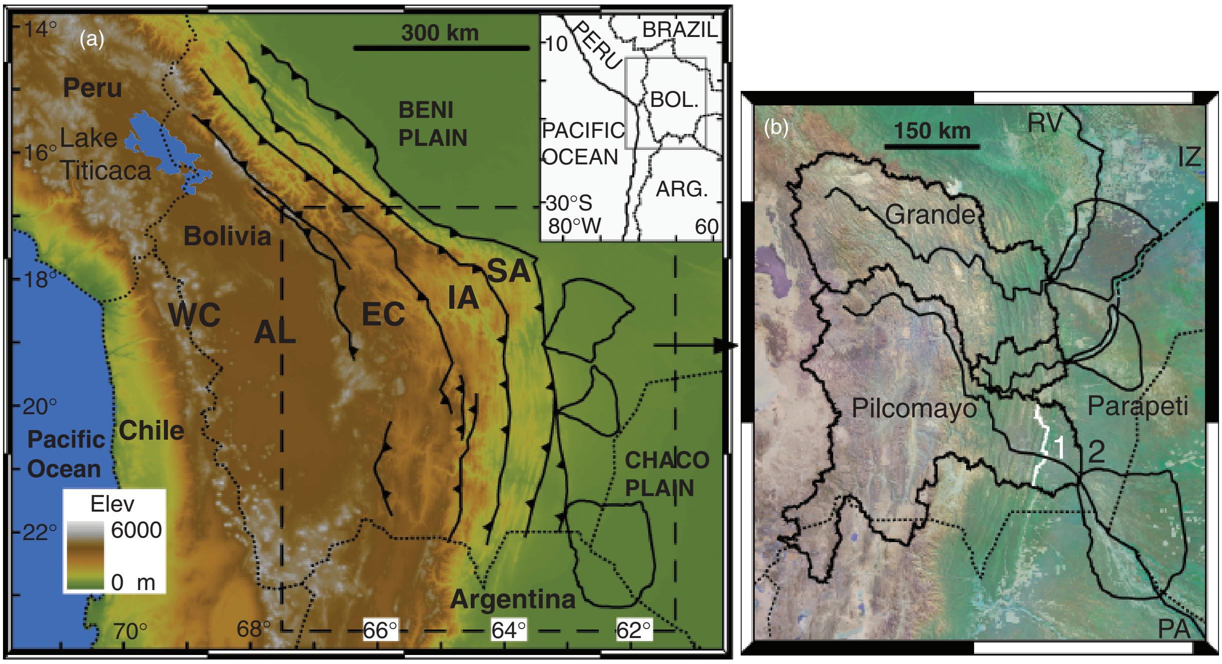

Fig. 2. Central Andean fold-thrust belt and Chaco foreland in Bolivia. (a) Topography (GTOPO30 1 km) and major tectonic zones (modified from McQuarrie, 2002; Uba *et al.*, 2006): WC, Western Cordillera; AL, Altiplano; EC, Eastern Cordillera; IA, Interandean zone; SA, Subandes. Megafans are outlined in black. Inset shows location in west-central South America. (b) Satellite image of study area draped over topography (SRTM 90 m) showing the Río Grande, Río Parapeti and Río Pilcomayo channels (solid lines where perennial, dashed where ephemeral), their drainage areas, and megafans. RV, Rio Viejo area; IZ, Izogog swamp; PA, Patino swamp; 1, white line representing the eastern basin edge of Pilcomayo 1 (Table 1); 2, black line representing the eastern basin edge of Pilcomayo 2 (Table 1) at the megafan apex (see text and Supporting Information for discussion).

ments since the late Oligocene (Uba *et al.*, 2006). Reconstructions of the widespread late Miocene San Juan del Oro (SJDO) erosion surface provide an unusual constraint on timing and volume of thrust belt erosion (Servant *et al.*, 1989; Gubbels, 1993; Gubbels *et al.*, 1993; Kennan *et al.*, 1997). Finally, source region erosion rates have been estimated across multiple spatial and temporal scales (e.g. Barnes & Pelletier, 2006 and references therein).

GEOLOGIC SETTING

Crustal shortening associated with Cenozoic Andean mountain building has resulted in a retroarc plateau, fold-thrust belt, and foreland basin system in western Bolivia (Fig. 2) (Jordan & Alonso, 1987; Isacks, 1988; Jordan, 1995; Kley, 1996, 1999; Allmendinger *et al.*, 1997; Horton & DeCelles, 1997; Jordan *et al.*, 1997; McQuarrie, 2002; DeCelles & Horton, 2003; McQuarrie *et al.*, 2005). The dominantly east-vergent fold-thrust belt steps down in structural and topographic elevation from the Altiplano to the Eastern Cordillera, Interandean zone, Subandes and Beni/Chaco plains (Kley, 1996; McQuarrie, 2002). Rocks involved in the deformation range from Palaeozoic marine siliciclastics to Mesozoic non-marine clastics and Cenozoic synorogenic deposits (McQuarrie, 2002 and references therein). In southern Bolivia, the fold-thrust belt is flanked on the west by the Altiplano basin and on the east by the Chaco plain (Fig. 2). The Altiplano is a low-relief, internally drained, intermontane depression (e.g. Placzek *et al.*, 2006). The Chaco plain is a low-relief, low-elevation slope thought to be the aggradational surface of the wedge-top and foredeep depozones of the modern foreland (Horton & DeCelles, 1997). The thrust belt is traversed by three large rivers, the Río Grande (or Guapay), Río Parapeti and Río Pilcomayo, which form fluvial megafans in the Chaco (Fig. 2b) (Horton & DeCelles, 2001). The relatively straight river courses across the Subandes suggest the rivers are antecedent from the late Miocene and hence the source drainages somewhat long lived. Megafan apexes begin at the frontal-most Subandes structure implying a more recent origin (Fig. 2b) (Horton & DeCelles, 2001).

Timing of initial thrust belt deformation ranges from late Eocene to late Oligocene (~27–40 Ma) with deformation concentrated in the Subandes since the early to late Miocene (~10–20 Ma) (Elger *et al.*, 2005; McQuarrie *et al.*, 2005, 2008; Ege *et al.*, 2007; Barnes *et al.*, 2008). Sediment deposition in the Chaco foreland commenced with the late Oligocene Petaca Formation and continues today with the Emborozú Formation (Uba *et al.* 2006). Structural, stratigraphic and geophysical data from southern Bolivia constrain the regional Neogene evolution, particularly in the Subandes (Baby *et al.*, 1992, 1995; Dunn *et al.*, 1995; Roeder & Chamberlain, 1995; Kley, 1996, 1999; Moretti *et al.*, 1996; Müller *et al.*, 2002; Uba *et al.*, 2005) and Chaco (Marshall *et al.*, 1993; Hulka *et al.*, 2006; Uba *et al.*, 2006).

SAN JUAN DEL ORO SURFACE

Here, we summarize age constraints and reconstructions of the SJDO erosion surface that we adopt to quantify the palaeo-drainage morphology and sediment volume removed from below the surface by Plio-Quaternary incision. The SJDO surface is identified by spatially correlative, remnant, low-relief surfaces at *ca*. 2000–3800 m elevations, which have been mapped throughout the Eastern Cordillera and Interandean zone of southern Bolivia (Fig. 3). The SJDO surface is a composite landform of (1) low-relief erosional uplands, (2) coalesced pediments and (3) an unconformity beneath undeformed Tertiary sediments and ignimbrites that is the stratigraphic equivalent to surface types 1 and 2 (Fig. 4) (Servant *et al.*, 1989; Gubbels *et al.*, 1993; Kennan *et al.*, 1995, 1997; Barke & Lamb, 2006). All surface types are subhorizontal, truncate deformed bedrock, decrease in elevation eastward, and are sometimes mantled by sediments up to 250 m thick with inter-bedded tuffs and fossiliferous layers (Gubbels *et al.*, 1993; Kennan *et al.*, 1995, 1997). Surveying the surfaces, $^{40}Ar/^{39}Ar$ dating of the tuffs, and ages of mammalian fossils bracketing the unconformity, show that the age of the SJDO is time-transgressive from ~12 to 3 Ma with incision beginning 3 ± 1.5 Ma (Gubbels, 1993; Gubbels *et al.*, 1993; Kennan *et al.*, 1995, 1997; Barke & Lamb, 2006). The lack of deformation and a dominantly ~10 Ma age for the SJDO surface suggests (a) cessation of deformation in the Eastern Cordillera and its migration eastward into the Subandes, and (b) 1.1–2.5 km of surface uplift has occurred in the region since surface formation (Figs 2 and 3) (Gubbels *et al.*, 1993; Kennan *et al.*, 1997; Barke & Lamb, 2006).

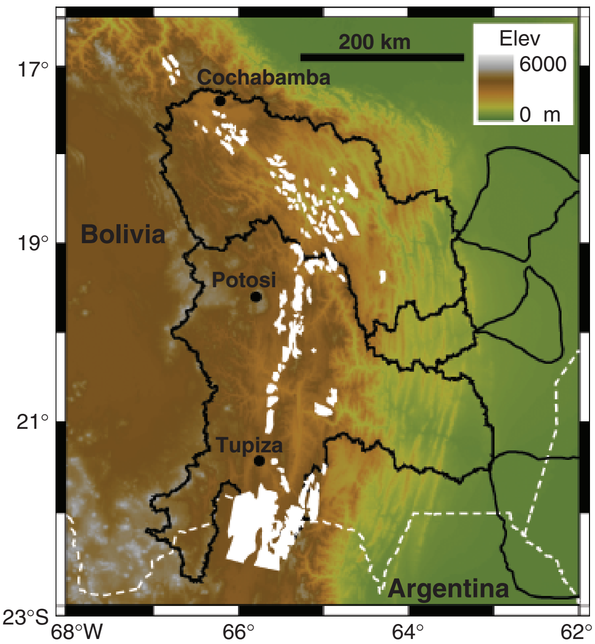

Fig. 3. Preserved remnants of the San Juan del Oro surface in southern Bolivia. Remnant surfaces are mapped in white (simplified from Kennan *et al.*, 1997) with the modern Grande, Parapeti and Pilcomayo basins and megafans outlined in black for comparison.

Two different models for SJDO surface formation characterize it as a pediment and palaeo-drainage base level, respectively. Gubbels and co-workers proposed a 'cut and fill' model for the SJDO surface whereby as deformation ceased, aggradation and pediment development began (Fig. 4) (Gubbels, 1993; Gubbels *et al.*, 1993). Eventually, incision isolated the surface remnants. In this model, the SJDO surface slopes down to the east from ~4.2 km elevation in the Eastern Cordillera to ~3 km in the Interandean zone over ~150 km (see Fig. 2.33 of Gubbels, 1993). This model suggests a regional gradient of ~0.46° and implicitly allows that the SJDO pediment was not ubiquitous and that intervening highlands existed (Fig. 4). Kennan and coworkers proposed that the SJDO surface represents the regional base level associated with two palaeo-drainage basins (Fig. 5a) (Kennan *et al.*, 1997; Kennan, 2000). This model suggests regional, upstream basin gradients of ~0.46° that decrease to ~0.23–0.27° in the downstream reaches. In both models, the preserved extent of the SJDO surface represents the minimum size of the drainage basin source area that supplied sediment to the foreland.

Key aspects of the SJDO surface relevant for quantifying a sediment budget include: (a) it formed ~10 Ma and (b) it experienced rapid incision at ~3 ± 1.5 Ma (Gubbels *et al.*, 1993; Kennan *et al.*, 1995, 1997; Barke & Lamb, 2006).

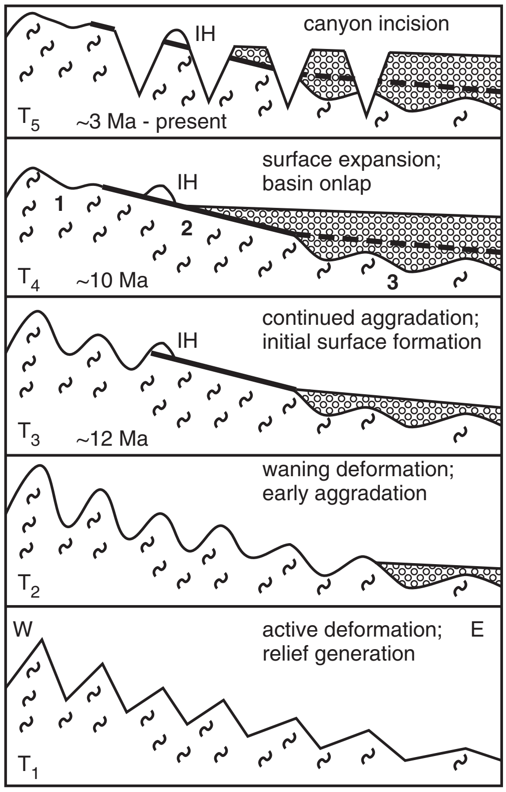

Fig. 4. Schematic of the cut and fill model for San Juan del Oro surface evolution in cross-section (modified from Fig. 4.1 of Gubbels, 1993). Five time steps are shown from pre-Miocene (T_1) to present (T_5) with absolute ages indicated where possible. Numbers 1–3 in T_4 indicate the three surface types as discussed in the text. IH, intervening highlands; W, west; E, east.

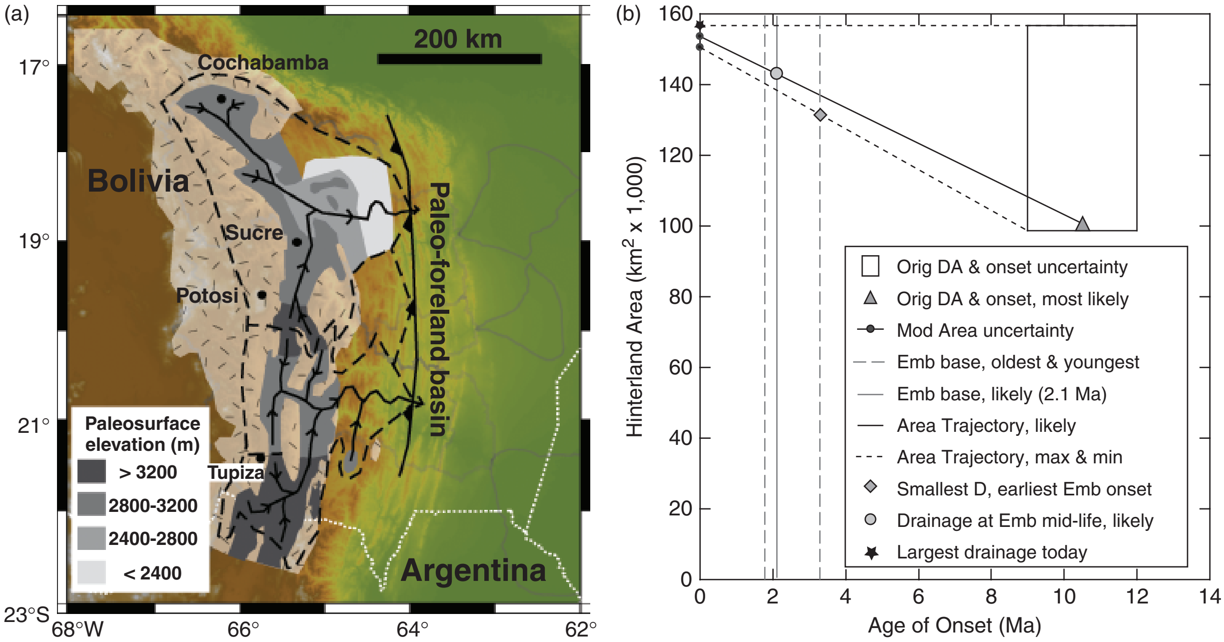

Fig. 5. The late Miocene (~10 Ma) palaeo-drainage model for San Juan del Oro surface evolution overlaying the modern topography. (a) Map of the palaeo-drainage basins (dashed black lines = boundaries, shaded regions are distributions of SJDO surface elevations today) from Kennan *et al.* (1997) with minor modifications at the outlet convergence to mimic the modern basins. Other features include local highlands (jackstraw pattern), river networks (solid black lines with arrows), mountain front (thrust fault) and palaeo-foreland basin (now occupied by the Subandes). Modern drainage basins and megafans (background grey lines) are shown for comparison. Two things to note; (1) the area between Potosi and Sucre used to be part of the palaeo-Grande basin, but has been captured by the Rio Pilcomayo (compare with Fig. 1b), and (2) the SJDO surface elevation range suggests typical regional gradients of 0.4–0.8% (Kennan *et al.*, 1997). (b) Various potential evolutionary trajectories between the palaeo- and modern drainages. Orig, original; DA, drainage area; Mod, modern; Emb, Emborozú Formation.

Additionally, an estimated 1–2 × 10^4 km^3 of material was eroded from the pre-existing topography above the palaeo-drainage base levels that together form the SJDO surface (Kennan *et al.*, 1997). All of this sediment was apparently transported out to the foreland (and possibly beyond) because neither (1) adequate local sinks exist in the EC or IA to store the estimated sediment nor (2) any major depositional hiatus exists in the Subandes source region between 12 and 3 Ma (Coudert *et al.*, 1993; Kennan *et al.*, 1997).

FORELAND SEDIMENTS

Isopachs constrain the spatio-temporal distribution of Oligocene to recent foredeep sediments in the Chaco plain (Uba *et al.*, 2006). The sedimentary unit most correlated with sediment exported from the thrust belt since the Plio-Quaternary is the Emborozú Formation (Uba *et al.*, 2006; their Fig. 15e). The Emborozú Formation is the currently depositing, sedimentary unit characterized by fluvial megafan-dominated conglomerates inter-bedded with sandstone and mudstone (Uba *et al.*, 2005). A seismic N5 interval is equivalent to the Emborozú Formation, which has a maximum thickness of ~1500 m at the mountain front and tapers rapidly eastward (Fig. 6) (Uba *et al.*, 2006). Beginning of Emborozú Formation deposition has been variously estimated at 3.3 Ma (Moretti *et al.*, 1996), 2.1 ± 0.2 Ma (Hulka, 2005) and 1.8 Ma (Echavarria *et al.*, 2003). The basal age of 2.1 ± 0.2 Ma is preferred (Uba *et al.*, 2006) because it agrees with the 1.8 Ma documented correlative strata in Argentina by Echavarria *et al.* (2003).

METHODS

We account for the sediment budget in the Andean fold-thrust belt and Chaco foreland across a range of scales: spatially, from the drainage basin and megafan to entire hinterland drainage and proximal foredeep; and temporally, from recent to the late Miocene–Pliocene. Here, we briefly outline the datasets and methods. Further details, particularly related to the definition and quantification of uncertainties, are available as Supporting Information.

We used ArcGIS™ 9.2 and the following datasets to estimate the modern morphology and area of the Río Grande, Río Parapeti and Río Pilcomayo catchments and megafans: 1 : 250 000 topographic maps from the Instituto Geografico Militar (IGM) in Bolivia, 15–150 m LANDSAT TM-7 satellite imagery, a hydrologically conditioned digital elevation model (HydroSHEDS: http://hydrosheds.cr.usgs.gov/), and digital topography derived from NASA's 2000 Shuttle Radar Topographic Mission (SRTM). All mapping and calculations reported were carried out in the Geographic and Universal Transverse Mercator (Zone 20 South) coordinate systems with the datum WGS84.

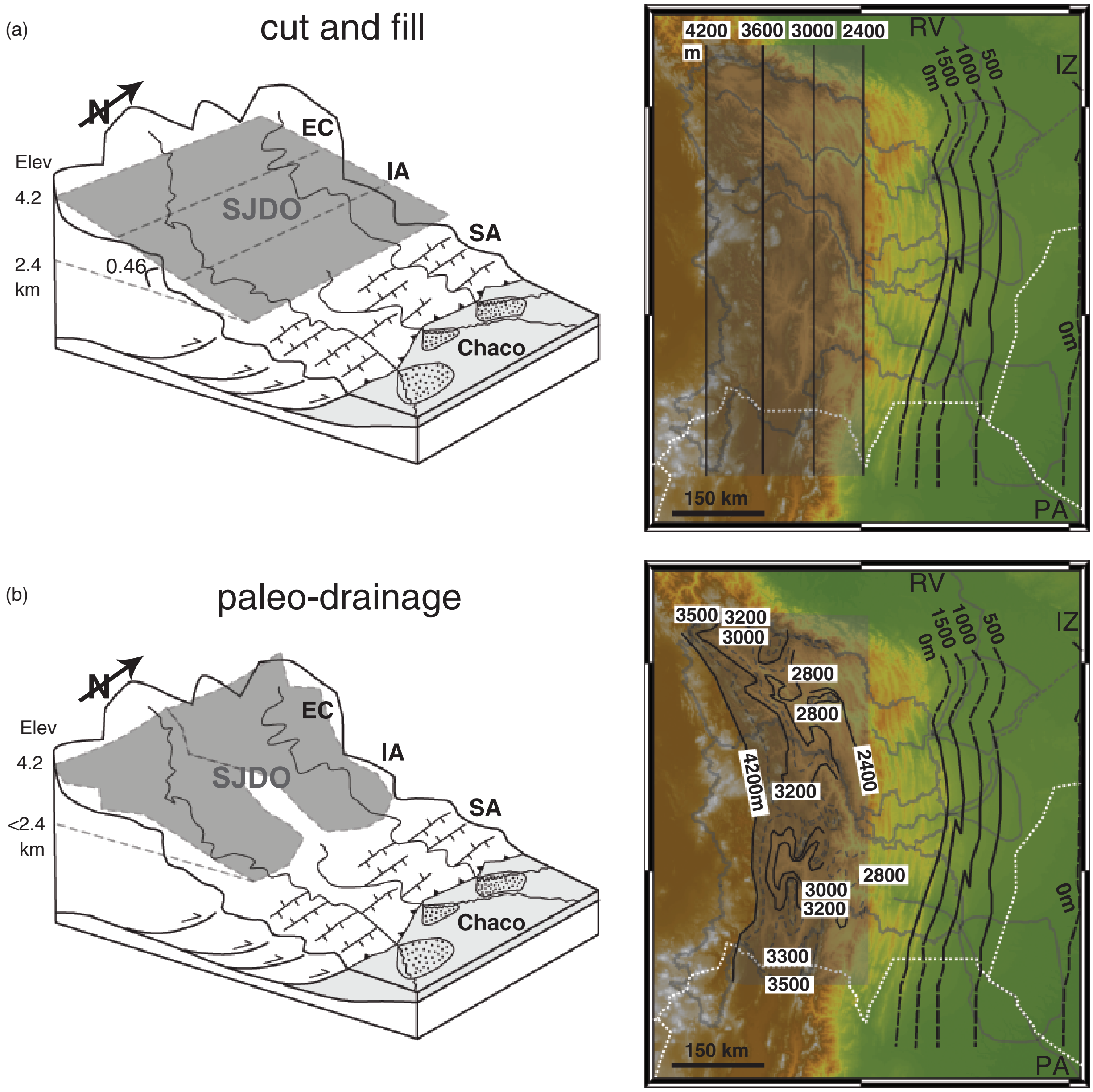

Fig. 6. San Juan del Oro (SJDO) surface reconstructions and Chaco basin isopachs in southern Bolivia. Contours (solid lines; dashed where inferred) used to recreate the SJDO surface before Plio-Quaternary incision. Foreland isopachs (dashed where inferred in this study) are for the ~2.1–0 Ma Emborozú Formation (from Uba *et al.* (2006); their Fig. 15e). Abbreviations are the same as in Fig. 2. Schematic block diagrams of the idealized SJDO surface reconstructed (left) and the distribution of elevation contours used to create the gridded surface (right) on top of the modern topography for the cut and fill (a) and palaeo-drainage (b) models. Idealized trellis drainage pattern shown for the Subandes. Grey-shaded region is the extent of the reconstructed SJDO surface in each model. Block diagram in B shows how basin slopes grade inward to the centre and eastward to the foreland. Contours in B are from Fig. 5 plus additional, inferred lines (grey dashed) where necessary.

We defined and mapped megafan margins by one or several of the following criteria; (1) at the transition from foreland-convex to mountain-front parallel contours, (2) the boundary between (a) well-defined distributary channels and their flanking overbank areas (both of which can be clearly linked back to the fan apex) and (b) inter-megafan areas (with drainages originating from the frontal anticlinal ridge, not from the fan apex), (3) systematic changes in local slope aspects and their magnitude and (4) consistent contrasts in colour, morphology and texture from 15 m satellite images artificially enhanced by topographic shading from multiple sun angles (criteria 2 and 3 after Horton & DeCelles, 2001; B. K. Horton, pers. comm., 2006).

We overlaid the palaeotopography associated with the SJDO surface reconstructions of Gubbels (1993) and Kennan *et al.* (1997) onto the modern topography in order to compare them. We created gridded surfaces corresponding to the reconstructed SJDO surfaces for both models to estimate the volume of material incised from below the surface by measuring the volume difference relative to the modern topography (Fig. 6). For the cut and fill model (Gubbels, 1993), we created a surface by interpolating between four N–S contours that span 66.5–64.4°W to 17–23°S. The contours have decreasing values from west to east of 4200, 3600, 3000 and 2400 m to replicate a regional gradient of 0.46°. This surface has a calculated mean slope of $0.46 \pm 0.06°$ (1σ). For the palaeo-drainage model (Kennan *et al.*, 1997), we created a surface by interpolating between contours tracing the distribution of regional palaeosurface elevations (compare Figs 5 and 6b). Additional contours were added for this interpolation to properly recreate the palaeotopographic highlands and intermediate palaeosurface elevations. However, the spatial extent of the contours was limited to that estimated by the palaeo-drainage reconstructions (Kennan *et al.*, 1997). The resultant surface slopes mimic the estimated values of 0.46–0.23°, but locally possess slopes of $< 0.2°$ in the downstream regions and $> 1°$ in very limited areas of the mid-to-upper reaches.

The nature and geometry of fluvial megafan basal surfaces have yet to be studied. Therefore, we calculated megafan volumes between the modern topographic surface and two alternate basal-surface geometries: (1) a horizontal, planar, basal surface equal in elevation to the minimum megafan surface elevation, and (2) a basal surface that is the mirror image of the fan surface about a horizontal plane of symmetry at the lowest elevation. Under assumption (1), the volume of the megafan is equal to (average elevation − lowest elevation) × surface area. Under assumption (2), the volume is just twice the value of assumption (1). Assumption (1) is a minimum estimate and assumption (2) is a more realistic estimate (see Supporting Information for further discussion).

We created a gridded surface corresponding to the base of the N5 seismic interval defined by isopachs (Uba *et al.*, 2006) in order to estimate the sediment volume in the foredeep. To encompass the entire study area, isopachs were extended parallel to the mountain front both north and south. We inferred the zero isopach to be parallel to the 500 m isopach and east of the Pilcomayo megafan margin because there are no data to constrain its location more specifically (Fig. 6).

RESULTS

Modern drainage areas

Drainage basin area estimates for the Grande, Parapeti and Pilcomayo are $59\,381 \pm 1188$, 7453 ± 149 and $86\,798 \pm 1736\ \mathrm{km}^2$, respectively (Table 1). These estimates are within 7–15% of those previously reported (Horton & DeCelles, 2001; Leier *et al.*, 2005) for reasons related to choice of basin outlet position and/or differences in map projection and datum (Table 1 and Supporting Information). For example, variation among area estimates using identical catchment boundaries, but different projections is ~10%. Minimum, maximum and average elevations, as well as relief, are also summarized in Table 1.

Palaeo-drainage areas

The palaeo-Río Grande and Río Pilcomayo drainage basins, as defined by the SJDO surface, may have covered

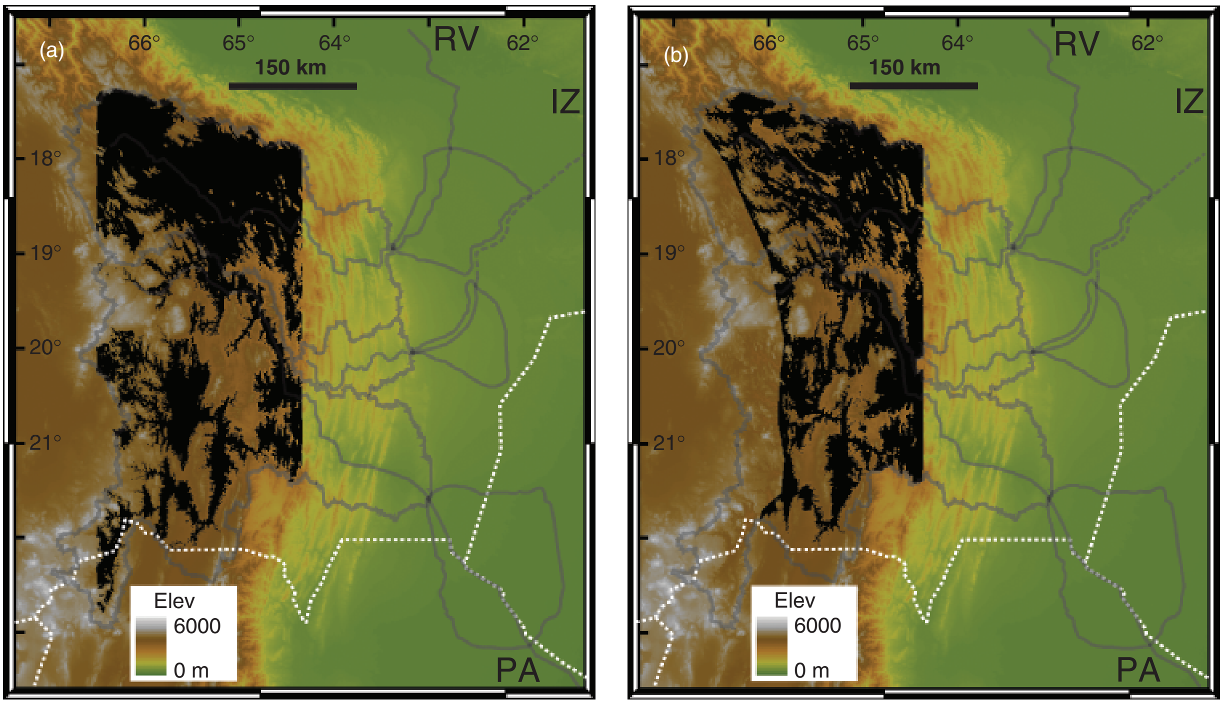

Fig. 7. Spatial distribution of Plio-Quaternary (~3–0 Ma) incision for both San Juan del Oro (SJDO) surface models. Black areas indicate volume loss when comparing the reconstructed SJDO surfaces with the modern topography for the cut and fill (a) and palaeo-drainage (b) models. Significantly less volume has been lost from the Grande basin in the palaeo-drainage model.

an area of $> \sim$100 000 km^2 at $\sim$10 Ma (Fig. 5a). Taking the palaeo-drainage model of the SJDO surface at face value, we estimate the size of the palaeo-Grande, Parapeti and Pilcomayo drainage basins (Fig. 5) to be 52 620, 9336 and 38 750 km^2, respectively (Table 1). Apparently, the palaeo-Grande basin was larger than the palaeo-Pilcomayo basin because the Potosi-Sucre area was subsequently captured by the Río Pilcomayo (compare Figs 2b and 5a). In total, the preserved remnants of the SJDO surface delineate a minimum drainage area of 100 706 km^2, which is roughly two-thirds of the modern surface area of the three drainage basins (Table 1). The modern drainage (Fig. 2b) represents the maximum area that could have been covered by the SJDO surface. Figure 5b shows the range of uncertainty in palaeo and modern area estimates and potential evolutionary trajectories between the two of them.

Volume excavated below the SJDO surface

We estimate 23 920–30 900 km^3 has been removed by incision from below the SJDO surface since 3 ± 1.5 Ma. Figure 7 shows regions that have experienced volume loss between the SJDO surface and the modern topography for both surface reconstruction models. The distribution of incision below both models is similar in the Pilcomayo basin. This reflects the fact that (1) the cut and fill model was based almost exclusively on remnants located in the Pilcomayo drainage (see Gubbels *et al.*, 1993; Fig. 1) and (2) most of the aerial extent of surface remnants is preserved there today (Fig. 3), providing most of the control for both models. Significantly less incision below the SJDO surface in the Grande basin is determined from the palaeo-drainage model because this model predicts a lower local base level

Table 1. Source and sink physical dimensions in southern Bolivia

	Grande	Parapeti	Pilcomayo (1)	Pilcomayo (2)	Total
Drainage Basin					
Maximum elevation (m)	4988	3303	5741	5741	
Minimum elevation (m)	442	631	389	320	
Relief (m)	4546	2672	5352	5421	
Average (m)	2631	1706	2851	2788	
Area (km^2)					
Horton & DeCelles (2001)	~70 000	~8000	~81 300	–	
Leier *et al.* (2005)	59 000	~8000	81 506	–	
This study	59 381	7453	80 832	86 798	153 632
This study error (± 2%)	± 1188	± 149	± 1617	± 1736	± 3073
~10 Ma	52 620	9336	–	38 750	100 706
Basin outlet, fan apex					
Modern long (°W)	63.4	63.19	63.47	63.01	
Modern latitude (°S)	18.91	20.02	21.27	21.56	
~10 Ma long (°W)	~64	~64	–	~64	
~10 Ma latitude (°S)	~18.5	~20	–	~21	
Megafans					
Maximum elevation (m)	575	646	–	360	
Minimum elevation (m)	299	384	–	198	
Relief (m)	276	262	–	162	
Average (m)	423	507	–	272	
Area (km^2)					
Horton & DeCelles (2001)	~12 600	~5800	–	~22 600	
Leier *et al.* (2005)	9944	6726	–	17 294	
This study	12 985	6142	–	22 511	
This study error (± 20%)	± 2597	± 1228	–	± 4502	
(Average-min) elevation (km)	0.124	0.123	–	0.074	
Volume (km^3)					
Max (area × 1.2 × average-min × 2)	3864	1813	–	3998	9675
Likely (area × average-min − 2)	3220	1511	–	3332	8063
Min (area × 0.8 × Average-min)	1288	604	–	1333	3225
Chaco Foredeep					
Area (km^2)					132 080
Error (± 2%)					± 2642
Volume of Emborozú Fm (km^3)					63 772
Error (± 20%)					± 12 754

1, pilcomayo basin boundary 1; 2, pilcomayo basin boundary 2 (see Fig. 2b). Max, maximum area estimate and mirror-image basal-surface assumption. Likely, area estimate and mirror-image basal-surface assumption. Min, minimum area estimate and planar-basal-surface assumption.

relative to the Pilcomayo basin (Fig. 5). The nature of the difference between the two models suggests the cut and fill surface represents an upper bound and the palaeo-drainage surface represents a lower bound on the volume of material removed. The results are reported this way.

Megafan areas

The fluvial megafans extend >150 km across the foredeep from their mountain-front apexes to their distal lobes. Total surface area of the megafans is $\sim$42 000 km^2, whereas the total surface area of the proximal Chaco foredeep is $\sim$132 000 km^2 (Table 1). We estimate the megafan surface areas to be 12 985, 6142 and 22 511 km^2 $\pm$ 20% for the Grande, Parapeti and Pilcomayo, respectively (Table 1 and Supporting Information). Our mapping criteria are sufficiently restrictive that the estimate of the Pilcomayo megafan is an order of magnitude less than the 210 000 km^2 reported by Iriondo (1993).

Megafan and foredeep basin fill volumes

Megafan volumes corresponding to the planar-basal-surface and mirror-image assumptions are reported in Table 1. The estimates range from 604 km^3 for the Parapeti megafan assuming a planar surface, to 3332 km^3 for the Pilcomayo megafan assuming a mirror image between the fan surface and the basal surface. The foredeep volume of the Emborozú Formation is 63 772 km^3 $\pm$ 20% (Table 1 and Supporting Information).

Denudation-rate estimates

Barnes & Pelletier (2006) compiled denudation-rate estimates from a variety of methods for southern Bolivia. Estimates range from 0.04 to 1.6 mm year^{-1} (= km Ma^{-1}) (Fig. 8). These estimates integrate sediment removal over temporal scales of 10^1–10^7 years and spatial scales from 10^0 to 10^5 km^2 (Fig. 9) (see Supporting Information for further discussion).

The relevant denudation rate for our source-to-sink calculation is an idealized average over the whole hinterland (10^5 km^2) and the whole depositional history of the Emborozú Formation (10^6 years) (see Supporting Information for additional discussion). Although observations span a range of values, the highest rates come from smaller spatial scales and larger temporal scales than the relevant analytic scale (Fig. 9). Observations that come from the relevant analytic scales (black oval in Fig. 9) fall into a much smaller range of 0.1–0.4 mm year^{-1}. The only observation that matches the relevant analytic spatial and temporal scale is $\sim$0.2 mm year^{-1} (grey circle in Fig. 9).

Sediment production and deposition estimates

Boundary conditions

This source-to-sink sediment budget starts with today and integrates back to the Plio-Quaternary ($\sim$3–0 Ma). The chronologic boundary is either initial incision into the SJDO surface or initial deposition in the Emborozú

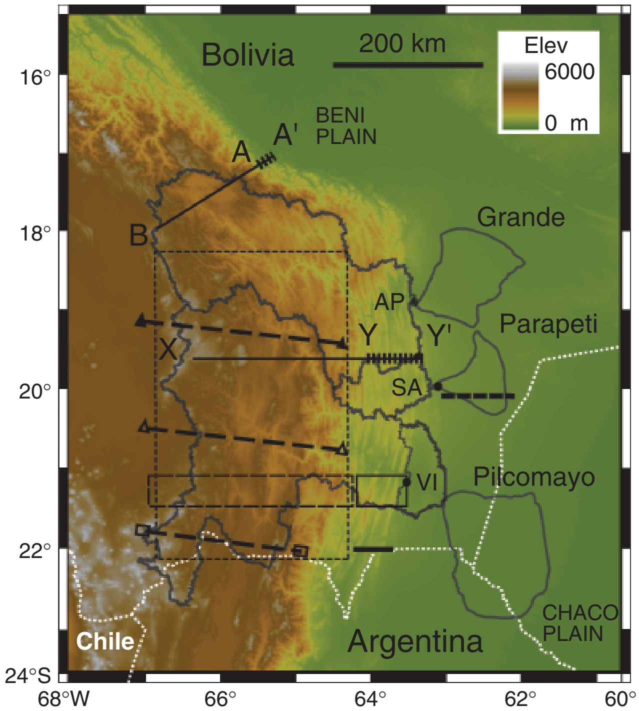

MAP KEY			
Symbol	Erosion rate (mm/yr)	Method	Time Span
A A'	**0.43-0.84**	x-section	0-15 or 20 Ma
B A'	**0.15-0.27**	x-section	0-40 Ma
	0.13-0.2	mass bal	0-2 or 3 Ma
AP	**0.89-0.93**	sed flux	years
	0.04-0.09	ES/DEM	0-10 Ma
Y Y'	**0.07-0.22**	x-section	0-15 or 20 Ma
X Y'	**0.08-0.16**	x-section	0-40 Ma
SA	**0.98-1.04**	sed flux	years
	0.13-0.27	seismic	0-2 or 3 Ma
	0.04-0.08	ES/DEM	0-10 Ma
	0.9-1.6	AFT	0-12 Ma
	0.1-0.6	AFT	10-40 Ma
	0.04-0.09	ES/DEM	0-10 Ma
	0.33	basin fill	0-5 Ma
VI	**0.33-0.35**	sed flux	years

Fig. 8. Map showing locations of erosion-rate estimates for the central Andean fold-thrust belt in southern Bolivia (modified from Barnes & Pelletier, 2006). Method, method used for calculating the estimate; Time Span, time span over which the erosion rate is averaged; sed flux, sediment-flux data with range of published data from Aalto *et al.* (2006) and Barnes & Pelletier (2006); AFT, apatite fission-track thermochronology; *x*-section, cross-section; mass bal, mass balance; ES/DEM, erosion surface and DEM analysis; seismic, seismic cross-sectional area; basin fill, basin fill rate.

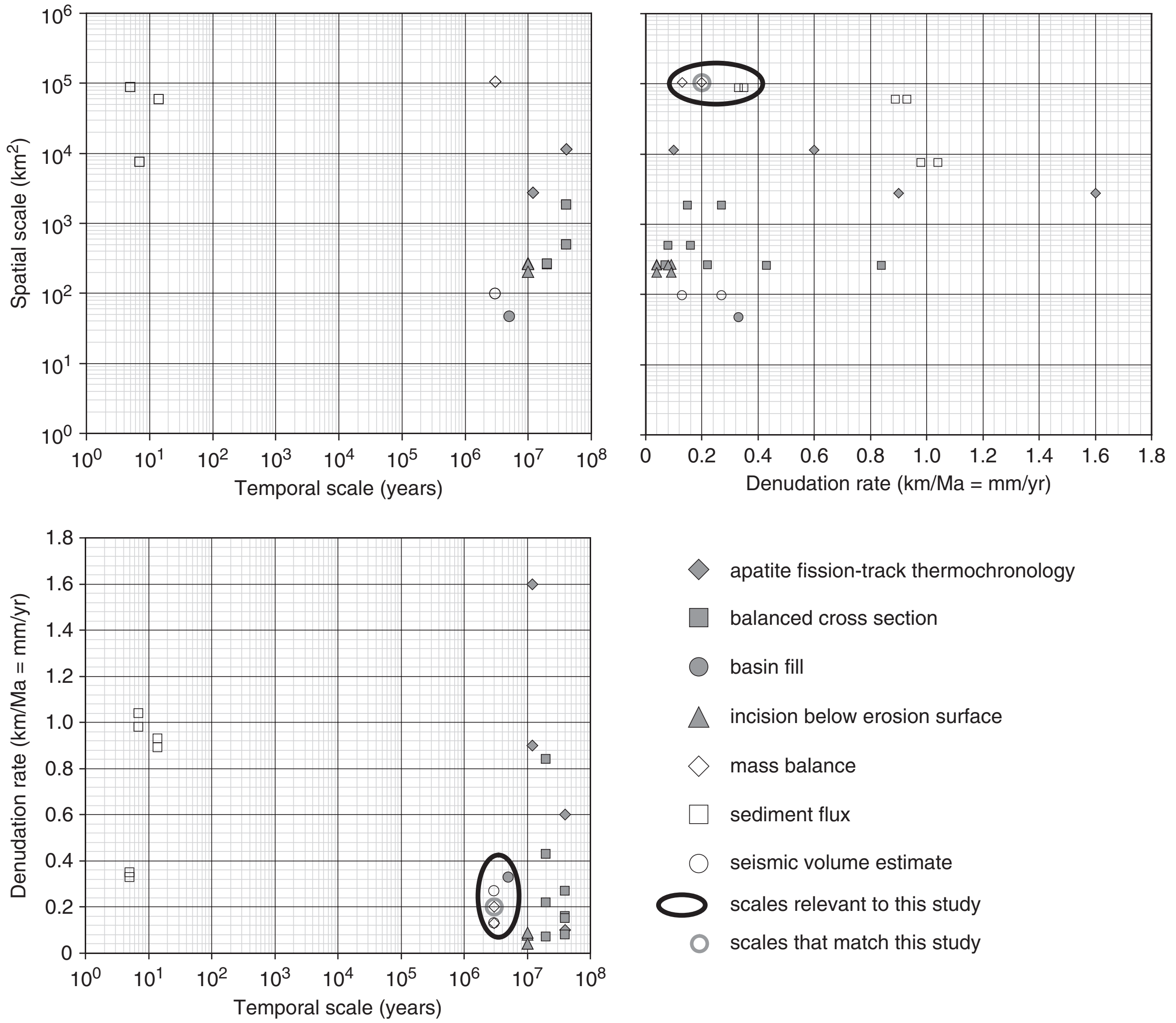

Fig. 9. Erosion-rate estimates vs. their integration in space and time for the central Andean fold-thrust belt in southern Bolivia (data from Barnes & Pelletier, 2006). Ovals highlight values that are both relevant (black) and specifically match (grey) the scale of this study.

Formation. In space, the budget starts with the modern landscape, bounded by the modern drainage divides of the Ríos Grande, Parapeti and Pilcomayo on the source side and by the zero-isopach of the Emborozú Formation on the sink side. The spatial boundary ends with the pre-incision SJDO surface and bordering highlands and the basal surface of the Emborozú Formation.

Volume balance

The source area sediment volume produced must be at least as large as the volume of sediment deposited in the Emborozú Formation. The maximum volume of sediments excavated from below the preserved area of the SJDO surface ($\sim$2.4–3.1 $\times$ $10^4\,km^3$) is smaller than the minimum volume of the Emborozú Formation ($\sim$5.1 $\times$ $10^4\,km^3$) (Table 1). Initiation of incision into the SJDO surface (4.5–1.5 Ma) overlaps with initial Emborozú Formation deposition (3.3–1.8 Ma) within error, but incision (most likely age 3.0 Ma) probably predates initial deposition (most likely age 2.1 Ma). The volume disparity between incision and deposition means that erosion from the intervening highlands and the drainage regions beyond the SJDO surface extent (Fig. 7) contributed at least $\sim$40–60% of the sediment to the Emborozú or $\sim$2–2.7 $\times$ $10^4\,km^3$ by volume.

Treatment of ions and pores

Exposed source-area bedrock is mostly Mesozoic and Palaeozoic siliciclastic sedimentary rock (e.g. McQuarrie, 2002). These rocks have some preserved porosity. Some fraction of the rocks is also lost to dissolution during conversion of bedrock to transportable sediment. We estimate that the volume lost to dissolved ions ($\sim$1–15%) plus the original rock porosity ($\leq$ 12%) is similar to the volume of void space among sedimentary particles deposited in the basin (16–32%) (see Supporting Information for quantitative justification). Thus, we treat gross volumes of denuded and deposited material as equivalent because the solid/void ratio is similar between source and sink.

Estimates

There are two paths for estimating sediment-production rates from the source area based on the data in this paper. First, we divided the volume of sediment excavated from beneath the SJDO surface by the time incision began. Table 2 summarizes the range of sediment-production rates calculated from the estimated volumes and time. Sediment-production rates range from 5316 to 20 600 km^3 Ma^{-1} with a middle value of 9137 km^3 Ma^{-1}. Second, we integrated linear denudation rates over the hinterland area. Table 2 also summarizes the sediment-production rates calculated from a range of denudation rates and potential hinterland areas. Denudation rates were chosen to uniformly cover (on a $\log_2$ scale) the range reported in Fig. 8. We picked areas from Fig. 5b to represent the smallest, likely, and largest regions that could have been encompassed by the drainage from the earliest initiation of Emborozú deposition to today. These sediment-production rates show a much wider range, from 5261 to 250 733 km^3 Ma^{-1} with a middle value of 57 215 km^3 Ma^{-1}.

There is only one path to estimate sediment-deposition rates. We divided the Emborozú Formation sediment volume by the time since deposition began. Sediment-deposition rates calculated from a range of estimated volumes and times are in Table 2. Rates range from 22 182 to 42 515 km^3 Ma^{-1} with a middle value of 30 368 km^3 Ma^{-1}. The deposition duration of 3.3 Ma is included for completeness, but is considered unlikely (see discussion in Uba *et al.* (2005)).

Reconciling the estimates

We calculated the minimum extra upland area required to produce the Emborozú sediment by subtracting the volume of SJDO surface excavation from the volume of the Emborozú then dividing by a linear denudation rate. The value is only a minimum because some SJDO surface-derived sediment might have been deposited elsewhere (e.g. in an older formation or bypassed downstream). Nevertheless, this exercise excludes denudation-rate estimates that are impossible for the relevant scale because they require more upland area than exists today. Table 3 summarizes the results within the ranges of rates, space and time constrained by observations. Space limits encompass the smallest total palaeo-drainage size (corresponding to the earliest onset of Emborozú deposition) to the largest possible modern drainage size (estimate plus error). Time limits were derived from the oldest potential onset of Emborozú deposition and the youngest possible onset of incision. Incision probably began earlier than the oldest onset of Emborozú deposition, but that case is not relevant to this calculation of minimum area. Table 3 rows are ordered by increasing mass flux required to fill the Emborozú. The results are shaded to indicate possibility: impossible (dark shading) because the combination of volumes and rates imply a hinterland area greater than the modern drainage, possible results (light shading) because they are within the range of potential hinterland areas, and certainly possible (no shading) results because they are smaller than the smallest drainage size.

Table 2. Potential Plio-Quaternary sediment production and deposition rates

Sediment-production rates (km^3 Ma^{-1})

Volume removed below SJDO (km^3)		Excavation duration (Ma) 1.5	3	4.5
Minimum	23 920	15 947	7973	5316
Likely	27 410	18 273	9137	6091
Maximum	30 900	20 600	10 300	6867

Hinterland denudation rates (km Ma^{-1})		Potential hinterland area (km^2) 131 517	143 037	156 708
Highest	1.6	210 428	228 859	250 733
Median sediment flux	1.0	131 517	143 037	156 708
Median AFT, high balanced cross-section	0.8	105 214	114 429	125 366
Low sediment flux	0.4	52 607	57 215	62 683
Median balanced cross-section	0.2	26 303	28 607	31 342
Low balanced cross-section, AFT	0.1	13 152	14 304	15 671
Lowest	0.04	5261	5721	6268

Sediment-deposition rates (km^3 Ma^{-1}) in the Emborozú Formation

Volume deposited (km^3)		Deposition duration (Ma) 1.8	2.1	2.3	3.3*
Minimum	51 018	28 343	24 294	22 182	15 460
Likely	63 772	35 429	30 368	27 727	19 325
Maximum	76 526	42 515	36 441	33 272	23 190

Middle values are shaded gray, see text for discussion.
*Values in this column unlikely, see text and Uba *et al.* (2005) for discussion.

Results indicate that any denudation rate <0.1 km Ma^{-1} is impossible as the average is over the complete (time, space) that generated the Emborozú sediments (Table 3). Denudation rates <0.2 km Ma^{-1} are impossible unless the volume of sediments in the Emborozú is near the low end of the likely range, and the onset of deposition is towards the old end of the likely range. Given the most likely volumes of SJDO surface excavation, Emborozú deposition and deposition duration, the average denudation rate should have been ≥ 0.2 km Ma^{-1}.

Modern sediment-production estimates

Boundary conditions

This source-to-sink sediment budget starts with today and integrates backward to the onset of modern megafan deposition. The budget starts with the modern landscape surface, bounded by the modern drainage divides of the

Table 3. Total hinterland area required (km^2) to supply deficient volume (Emborozu – excavation below SJDO)*

	Excavated below SJDO (km^3)	Observed in Emborozú (km^3)	Extra volume required (km^3)	Excavation duration (Ma)	Production rate of extra volume (km^3 Ma^{-1})	Potential denudation rates (km Ma^{-1} = mm yr^{-1}): Highest 1.6	Median sediment flux 1.0	Median AFT, high balanced cross-section 0.8	Low sediment flux 0.4	Median balanced cross-section 0.2	Low balanced cross-section, AFT 0.1
	30 900	51 018	20 118	3.3	6096	102 500	104 786	106 310	113 930	129 171	159 652
	27 410	51 018	23 608	3.3	7154	103 161	105 843	107 632	116 574	134 459	170 228
	23 920	51 018	27 098	3.3	8211	103 822	106 901	108 954	119 218	139 747	180 804
	30 900	51 018	20 118	2.1	9580	104 677	108 269	110 664	122 639	146 589	194 488
	30 900	63 772	32 872	3.3	9961	104 915	108 651	111 141	123 593	148 496	198 302
	27 410	63 772	36 362	3.3	11 019	105 576	109 708	112 463	126 237	153 784	208 878
	27 410	51 018	23 608	2.1	11 242	105 716	109 931	112 742	126 794	154 898	211 107
	23 920	63 772	39 852	3.3	12 076	106 237	110 766	113 785	128 881	159 071	219 453
	23 920	51 018	27 098	2.1	12 904	106 754	111 593	114 819	130 949	163 208	227 726
	30 900	51 018	20 118	1.5	13 412	107 072	112 101	115 454	132 219	165 748	232 807
	30 900	76 526	45 626	3.3	13 826	107 331	112 516	115 972	133 255	167 821	236 951
	27 410	76 526	49 116	3.3	14 884	107 992	113 573	117 294	135 899	173 108	247 527
	30 900	63 772	32 872	2.1	15 653	108 473	114 343	118 256	137 823	176 956	255 223
	27 410	51 018	23 608	1.5	15 738	108 526	114 428	118 363	138 036	177 382	256 074
	23 920	76 526	52 606	3.3	15 941	108 653	114 631	118 616	138 543	178 396	258 103
	27 410	63 772	36 362	2.1	17 315	109 512	116 005	120 334	141 978	185 266	271 842
	23 920	51 018	27 098	1.5	18 065	109 980	116 755	121 271	143 852	189 015	279 340
	23 920	63 772	39 852	2.1	18 977	110 550	117 667	122 411	146 133	193 575	288 461
	30 900	76 526	45 626	2.1	21 727	112 269	120 417	125 848	153 007	207 324	315 958
	30 900	63 772	32 872	1.5	21 915	112 386	120 604	126 083	153 476	208 263	317 836
	27 410	76 526	49 116	2.1	23 389	113 308	122 078	127 926	157 162	215 633	332 577
	27 410	63 772	36 362	1.5	24 241	113 841	122 931	128 991	159 293	219 896	341 103
	23 920	76 526	52 606	2.1	25 051	114 346	123 740	130 003	161 316	223 943	349 196
	23 920	63 772	39 852	1.5	26 568	115 295	125 258	131 900	165 110	231 530	364 370
	30 900	76 526	45 626	1.5	30 418	117 701	129 107	136 712	174 734	250 778	402 866
	27 410	76 526	49 116	1.5	32 744	119 155	131 434	139 620	180 550	262 411	426 132
	23 920	76 526	52 606	1.5	35 071	120 609	133 761	142 528	186 367	274 044	449 399
Min	23 920	51 018	20 118	1.5							
Max	30 900	76 526	52 606	3.3		Upper			Lower		
Likely	27 410	63 772	36 362	2.1		Limit = 156 708 km^2			Limit = 131 517 km^2		

*Minimum area of preserved SJDO surface = 98 690 km^2; source areas required to supply deficit = extra vol production rate/denudation rate+98 690; dark shading, impossible results; light shading, possible results; no shading, certainly possible results; see Fig. 8 for abbreviations.
Outlined row is most likely result based on best combination of time and amount of excavated sediment below the SJDO and observed in the Emborozú Formation.

Grande, Parapeti and Pilcomayo rivers in the source, and bounded by the megafan extents in the sink.

The megafan sediment volume is probably equal to, or slightly less than, the volume produced in the source area for the following reasons. Very little surface water escapes the Chaco foredeep because the Río Parapeti and Pilcomayo terminate into swamps just downstream of their megafans and the Río Grande stalls as it bifurcates into small channels, drops sediments in the adjacent floodplains in the Río Viejo area beyond the megafan margin, and consequently severs its connection to the Río Paraguay (Fig. 2b) (Iriondo, 1984; Iriondo, 1993; Horton & DeCelles, 2001). In particular, the Río Pilcomayo presently deposits such a sediment excess that it blocks its own channel, floods its levees and spills into nearby swamps (Wilkinson *et al.*, 2006). Furthermore, tectonic depressions, vegetative-debris accumulations and abandoned channels facilitate water and sediment ponding in lakes both on and around the megafans (Iriondo, 1993; Wilkinson *et al.*, 2006). Finally, it is estimated that most of the Río Pilcomayo sediment load is trapped in the Chaco plain before joining the Parana river (Latrubesse *et al.*, 2005). The Supporting Information outlines observations that suggest the megafans themselves might not be entirely closed systems.

Sediment production

Integrating a linear denudation rate over the modern drainage area yields the modern sediment-production rate. Table 4 summarizes sediment-production rates calculated from a range of denudation rates and measured drainage areas. Denudation rates were chosen to cover the range reported with particular emphasis on rates estimated from the basin outlet on each of the rivers: 0.89–0.93 mm year^{-1} for the Grande (point AP in Fig. 8), 0.98–1.04 mm year^{-1} for the Parapeti (point SA in Fig. 8), and 0.33–0.35 mm year^{-1} for the Pilcomayo (point VI in Fig. 8). The highest rate used represents the highest observed rate throughout the Neogene (apatite fission-track thermochronology) whereas the lowest rate is the lowest possible calculated in Table 3. For each river, the best sediment-production rate estimate (shading) is based on the most likely drainage size and the measured denudation rate for that drainage.

Age of megafan initiation

If all sediment produced in the drainages is deposited on the megafans, as observations documented above suggest, then onset of modern megafan deposition can be estimated by dividing the megafan sediment volume by the rate of sediment production. Table 5 summarizes the results of this calculation with rate and volume ranges constrained by observation for each megafan and their aggregate.

For most likely values for drainage area, sediment delivery and megafan volume, estimated age of megafan initiation varies considerably from 52–55 ka for the Grande, to 110–116 ka for the Pilcomayo, and 218–228 ka for the Parapeti (Table 5 and Supporting Information). It is possible that this result is correct and megafan initiation is diachronous. Alternatively, modern denudation rates may be inaccurate estimates of the average rate since the (common?) initiation time of the megafans because they are based on only a few years, compared with the hundreds of

Table 4. Potential sediment-production rates from the modern landscape (km^3 Ma^{-1})

Drainage area (km^2)		**Observed denudation rates (km Ma^{-1} = mm yr^{-1})** Neogene highest 1.60	Grande highest 1.04	Grande lowest 0.98	Parapeti highest 0.93	Parapeti lowest 0.89	Neogene median 0.80	Pilcomayo highest 0.35	Pilcomayo lowest 0.33	Neogene lowest 0.20
Grande										
Maximum	60 569	96 910	62 991	59 357	56 329	53 906	48 455	21 199	19 988	12 114
Likely	59 381	95 010	61 756	58 193	55 224	52 849	47 505	20 783	19 596	11 876
Minimum	58 193	93 109	60 521	57 030	54 120	51 792	46 555	20 368	19 204	11 639
Parapeti										
Maximum	7602	12 163	7906	7450	7070	6766	6082	2661	2509	1520
Likely	7453	11 925	7751	7304	6931	6633	5962	2609	2459	1491
Minimum	7304	11 686	7596	7158	6793	6501	5843	2556	2410	1461
Pilcomayo										
Maximum	88 534	141 654	92 075	86 763	82 337	78 795	70 827	30 987	29 216	17 707
Likely	86 798	138 877	90 270	85 062	80 722	77 250	69 438	30 379	28 643	17 360
Minimum	85 062	136 099	88 465	83 361	79 108	75 705	68 050	29 772	28 070	17 012
Total										
Maximum		250 727	162 973	153 571	145 735	139 467	125 364	54 847	51 713	31 341
Likely		245 811	159 777	150 559	142 878	136 732	122 906	53 771	50 699	30 726
Minimum		240 895	156 582	147 548	140 020	133 998	120 447	52 696	49 685	30 112

Shading, best sediment-production rate estimate.

ka over which the megafans must have been accumulating. If we apply the median denudation rate observed across the entire Neogene to the total volume of sediments in all megafans, onset of deposition would be $\sim$66 ka. Table 5 essentially presents a series of hypotheses about the age of the modern Chaco megafans that can be tested by dating the actual basal surface. Radiocarbon or pollen ages from relatively shallow boreholes could provide the necessary information.

DISCUSSION AND IMPLICATIONS

Sediment production volumes through time and space

Estimated sediment volumes have implications for erosion variability through time and the distribution of sediment production within the source region. The *ca*. 1000 m relief between the SJDO surface and intervening highlands led Kennan *et al*. (1997) to estimate that $\sim$1–2 $\times$ 10^4 km^3 was excavated from the original palaeotopography to make the SJDO surface presumably before $\sim$10 Ma. Since $\sim$2–3 Ma, a minimum of $\sim$5.1 $\times$ 10^4 km^3 has been deposited into the Emborozú Formation, of which at least $\sim$40–60% (2.4–3.1 $\times$ 10^4 km^3) came from below the SJDO surface via incision. Although, we cannot quantify the source area extent at any point before SJDO formation, we speculate relative denudation rates were low for some time period before $\sim$10 Ma because the sediment volume produced was only $\sim$20–40% of the volume deposited in the last 3 Myr. This is already implied because most of the long-term ($>$10 Myr) averaged denudation rates are $<$0.4 mm year^{-1} (Fig. 9), and we already demonstrated they were most likely $\geq$ 0.4 mm year^{-1} during the Plio-Quaternary.

Comparison of estimated sediment volumes between source and sink over the last 2–3 Myr shows at least $\sim$40–60% came from incision into the SJDO surface. The remainder must have come from some combination of the intervening highlands and drainage areas outside the current SJDO surface extent. In map view (Fig. 7), the largest source areas not accounted for by SJDO incision are the modern Subandes and the intervening highlands. The Subandes probably contributed to the Emborozú Formation, but sediments probably can get trapped locally in the Tertiary piggyback basins before reaching the perennial Grande, Parapeti and Pilcomayo trunk rivers. The best candidate source might be the intervening highlands because they extend over significant areas and exhibit the steepest slopes.

Plio-Quaternary to modern denudation rates

Measurements of denudation rates, drainage areas and volumes of sediment produced or deposited are inherently imprecise. No singular observation, or even a range of observations on a single feature, can be considered accurate

Table 5. Potential age (Ma) of megafan initiation

		Potential sediment production rates from the modern landscape (km^3 Ma^{-1})			
		Absolute highest	High end of likely	Low end of likely	Absolute lowest
Megafan volume (km^3)		96 910	61 756	58 193	11 639
Grande					
Maximum	3864	0.040	0.063	0.066	0.332
Likely	3220	0.033	0.052	0.055	0.277
Minimum	1288	0.013	0.021	0.022	0.111
		Absolute highest	High end of likely	Low end of likely	Absolute lowest
		12 163	6931	6633	1461
Parapeti					
Maximum	1813	0.149	0.262	0.273	1.241
Likely	1511	0.124	0.218	0.228	1.034
Minimum	604	0.050	0.087	0.091	0.414
		Absolute highest	High end of likely	Low end of likely	Absolute lowest
		141 654	30 379	28 643	17 012
Pilcomayo					
Maximum	3998	0.028	0.132	0.140	0.235
Likely	3332	0.024	0.110	0.116	0.196
Minimum	1333	0.009	0.044	0.047	0.078
		Absolute highest	Neogene median		Absolute lowest
		250 727	122 906		30 112
All megafans					
Maximum	9675	0.039	0.079		0.321
Likely	8063	0.032	0.066		0.268
Minimum	3225	0.013	0.026		0.107

Shading, best sediment-production rate estimate.

in isolation. Observations can only be evaluated based on their internal consistency. Our analysis demonstrates that estimates of denudation $<0.1\,\mathrm{km\,Ma^{-1}}$ cannot (and estimates $<0.2\,\mathrm{km\,Ma^{-1}}$ probably do not) characterize the entire Bolivian-Andes hinterland of the Chaco foreland over the Plio-Quaternary (last 2–3 Myr) even though observations demonstrate that such rates may be locally viable (Fig. 8). Modern estimates suggest the Pilcomayo basin erodes at a rate ($0.34\,\mathrm{mm\,year^{-1}}$) near the minimum that characterized the Plio-Quaternary. In contrast, both the Grande and Parapeti basin rates (0.91 and $1.01\,\mathrm{mm\,year^{-1}}$) are significantly higher (Fig. 8). This variation in erosion rates could be the result of the general southward aridification (e.g. Barnes & Pelletier, 2006), anthropogenic effects, and/or sediment discharge variations resulting from the type of dominant erosion process and precipitation storminess (e.g. Fuller *et al.*, 2003).

Evolution of topography

Topographic evolution can be better understood by determining the amount and rate of morphologic change across different spatial and temporal scales. Here, we use the physical dimensions determined in this study to comment on central Andean fold-thrust belt and Chaco foreland topographic variations over the late Miocene–Quaternary (last $\sim$10 Myr).

The Grande, Parapeti and Pilcomayo basins collectively expanded by $\sim$50% from $\sim$100 000 to $\sim$150 000 km^2 since $\sim$10 Ma (Table 1). Migration of the drainage divide westward was $\sim$100 km since $\sim$10 Ma as was the migration of the drainage outlet eastward (Fig. 5). This migration rate of $10\,\mathrm{mm\,year^{-1}}$ is similar to locally estimated rates of thrust belt propagation (6–8 $\mathrm{mm\,year^{-1}}$), shortening ($\sim$4–8 $\mathrm{mm\,year^{-1}}$) and foreland basin migration

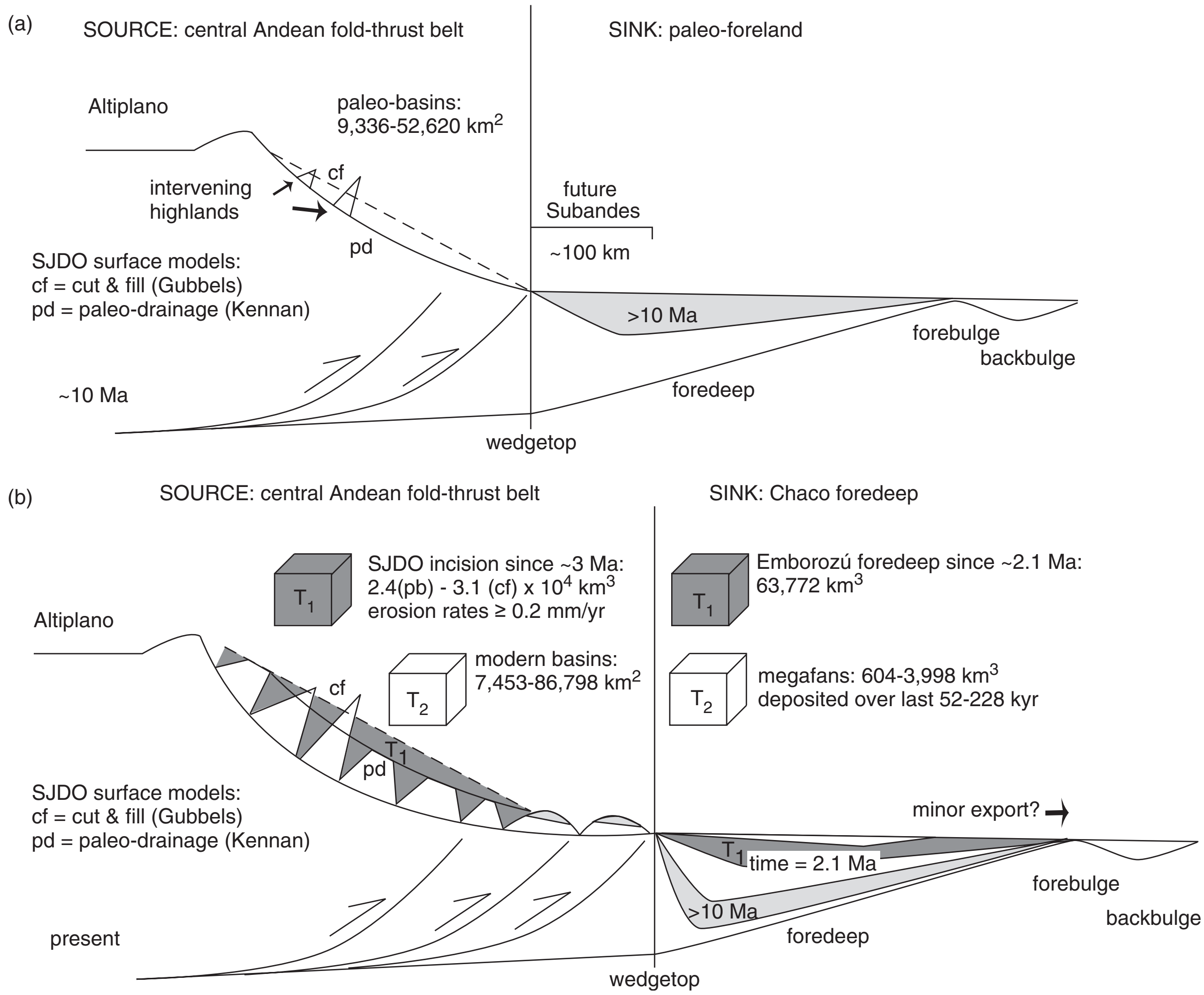

Fig. 10. Schematic central Andean fold-thrust belt and Chaco foreland basin system sediment budget in cross-section at $\sim$20°S. cf, cut and fill model surface representation (dashed line in source); pd, palaeo-drainage surface representation (solid concave up line in source). (a) Source and sink features during peak San Juan del Oro (SJDO) formation at $\sim$10 Ma before incision. (b) Source and sink features after incision at present. Time slice T_1 is the Plio-Quaternary to recent ($\sim$2 or 3–0 Ma) represented by the volume eroded by incision into the SJDO surface in the source and deposited within the Emborozú Formation in the sink, respectively. Time slice T_2 is very recent time ($\sim$230–0 ka) represented by the modern drainage areas and the megafan volumes in the foreland, respectively. Additional source region solid lines represent the modern maximum (jagged line) and minimum (lowest line) topography.

($\sim$13 mm year^{-1}) (McQuarrie *et al*., 2005; Barnes *et al*., 2008). Westward, headward erosion, stream piracy and eastward drainage expansion into the Subandes probably contributed to drainage basin growth. In particular, stream piracy by the Río Pilcomayo of the Sucre/Potosi region probably contributed the most to the Pilcomayo basin's growth of $\sim$115% from $\sim$40 000 to $\sim$87 000 km^2 (Table 2). Despite the area lost to the Pilcomayo, the Grande basin still grew in overall size by almost 10%. Finally, the Parapeti basin actually decreased in size by $\sim$15% probably via the encroachment of the two larger basins on either side of it. These data suggest that large (10^{4-5} km^2) drainages in (potentially protracted) semi-arid climates still evolve substantially over 10 Myr time frames.

The modern fluvial megafans are estimated to be up to $\sim$228 kyr old (Table 5). Unfortunately, to the best of our knowledge, no studies have estimated the age of any other modern megafans for comparison. Regardless, the $\sim$228 kyr age suggests that large sediment bodies can be dispersed over distances of >200 km across low-sloped (mostly $<0.35°$) regions rather rapidly even in semi-arid climates. Furthermore, the currently active megafans represent only a small portion (in either time or sediment volume) of the most recent seismically resolvable sedimentation history in the basin. In fact, sedimentary evidence suggests the Subandes megafans have existed for the last $\sim$8 Ma (Uba *et al*., 2007).

Thrust belt-foreland geodynamics

Thrust belt deformation and erosion are dynamically coupled to their associated foreland basin systems via deformation, foreland flexure and erosion (e.g. DeCelles & DeCelles, 2001). Models of this coupling predict that regions of reduced erosion are characterized by wedge growth, a wide, rapidly propagating thrust belt with dominantly wedgetop deposition and an underfilled foredeep, whereas regions of enhanced erosion possess wedge recycling, a narrow thrust belt with more constant width, and dominantly foredeep deposition in a wide and largely filled foreland (Simpson, 2004, 2006). These predictions are, to first-order, consistent with the central Andean fold-thrust belt where observations mentioned above suggest the dry, southern Chaco foredeep is basically underfilled and the wet, northern Beni foredeep is overfilled because $\sim$50% of the sediment bypasses it and enters the Amazon (Fig. 2) (Horton, 1999; Aalto *et al*., 2006; Barnes & Pelletier, 2006). Unfortunately, the models have only been developed for the general case. They could be tested by calibrating them to specific regions and constraining the surface process parameters with such datasets as those presented here.

SUMMARY

Figure 10 schematically illustrates the central Andean thrust belt-Chaco foreland basin system sediment budget presented here. Selected, important values derived throughout this study are indicated. Comparison of Figs 1 and 10 illustrates the contrast between the idealized and our applied thrust belt-foreland system sediment budget analysis.

ACKNOWLEDGEMENTS

Financial support was provided to J. Barnes by an ExxonMobil summer internship and NSF grant EAR 0409289 to T. A. Ehlers. We thank Bob Brovey for providing the enhanced satellite images. This paper benefited from early discussions with Brian Horton, Lorcan Kennan and Peter DeCelles, and very thorough reviews by Kennan, an anonymous reviewer, and editor DeCelles.

Supporting Information

Additional Supporting Information may be found in the online version of this article:

Appendix S1: Details on some of the methodologies and uncertainties presented in the main text.

Please note: Blackwell Publishing is not responsible for the content or functionality of any supporting materials supplied by the authors. Any queries (other than missing material) should be directed to the corresponding author for the article.

REFERENCES

Aalto, R., Dunne, T. & Guyot, J.L. (2006) Geomorphic controls on Andean denudation rates. *J. Geol.*, **114**, 85–99.

Allen, P.A. (2008) From landscapes into geological history. *Nature*, **451**, 274–276.

Allmendinger, R.W., Jordan, T.E., Kay, S.M. & Isacks, B.L. (1997) The evolution of the Altiplano-Puna Plateau of the Central Andes. *Annu. Rev. Earth Planet. Sci.*, **25**, 139–174.

Babault, J., van den Driessche, J., Bonnet, S., Castelltort, S. & Crave, A. (2005) Origin of the highly elevated Pyrenean peneplain. *Tectonics*, **24**, doi: 10.1029/2004TC001697.

Baby, P., Herail, G., Salinas, R. & Sempere, T. (1992) Geometry and kinematic evolution of passive roof duplexes deduced from cross section balancing; example from the foreland thrust system of the southern Bolivian subandean zone. *Tectonics*, **11**, 523–536.

Baby, P., Limachi, R., Moretti, I., Mendez, E., Oller, J., Guiller, B. & Specht, M. (1995) Petroleum system of the northern and central Bolivian sub-Andean zone. In: *Petroleum Basins of South America* (Ed. by A.J. Tankard, R. Suarez & H.J. Welsink), *Am. Assoc. Petrol. Geol. Mem.*, **62**, 445–458.

Barke, R. & Lamb, S. (2006) Late Cenozoic uplift of the Eastern Cordillera, Bolivian Andes. *Earth Planet. Sci. Lett.*, **249**, 350–367.

Barnes, J.B., Ehlers, T.A., McQuarrie, N., O'Sullivan, P.B. & Tawackoli, S. (2008) Thermochronometer record of central Andean Plateau growth, Bolivia (19.5°S). *Tectonics*, TC3003, doi: 10.1029/2007TC002174.

Barnes, J.B. & Pelletier, J.D. (2006) Latitudinal variation of denudation in the evolution of the Bolivian Andes. *Am. J. Sci.*, **306**, 1–31.

Beaumont, C., Kooi, H. & Willett, S. (2000) Coupled tectonic-surface process models with applications to rifted margins and collisional orogens. In: *Geomorphology and Global Tectonics* (Ed. by M. Summerfield), pp. 29–55. John Wiley & Sons, Chichester, UK.

Bonnell, L.M. & Lander, R.H. (2003) Reservoir quality prediction in deep water to tight gas sandstones using a process/stochastic modeling approach. *Am. Assoc. Petrol. Geol. Bull.*, **87**, AAPG Distinguished Lectures.

Bray, A.A., Lander, R.H., Watkins, C.A., Lowrey, C.J. & Owen, M.Anonymous (2000) Characterisation and prediction of clastic reservoir quality; an integrated model for use in exploration, appraisal and production projects. *Am. Assoc. Pet. Geol. Bull.*, **1408**.

Burgess, P.M. & Allen, P.A. (1996) A forward-modelling analysis of the controls on sequence stratigraphical geometries. *Geol. Soc. Lond. Spec. Publ.*, **103**, 9–24.

Clark, M.K., Royden, L.H., Whipple, K.X., Burchfiel, B.C., Zhang, X. & Tang, W. (2006) Use of a regional, relict landscape to measure vertical deformation of the eastern Tibetan Plateau. *J. Geophys. Res.*, **111**, doi: 10.1029/2005JF000294.

Clevis, Q., de Boer, P. & Wachter, M. (2003) Numerical modelling of drainage basin evolution and three-dimensional alluvial fan stratigraphy. *Sediment. Geol.*, **163**, 85–110.

Clevis, Q.J.W.A. (2003) Three-dimensional modelling of thrust-controlled foreland basin stratigraphy. Doctoral Thesis, Universiteit Utrecht, Utrecht.

Clift, P., Gaedicke, C., Edwards, R., Lee, J. II, Hildebrand, P., Amjad, S., White, R.S. & Schlueter, H.-U. (2002) The stratigraphic evolution of the Indus Fan and the history of sedimentation in the Arabian Sea. *Mar. Geophys. Res.*, **23**, 223–245.

Clift, P.D. (2006) Controls on the erosion of Cenozoic Asia and the flux of clastic sediment to the ocean. *Earth Planet. Sci. Lett.*, **241**, 571–580.

Coudert, L., Sempere, T., Frappa, M., Viquier, C. & Arias, R. (1993) Subsidence and crustal flexure Evolution of the Neogene Chaco Foreland Basin. Third International Symposium on Andean Geodynamics, Oxford, extended abstracts, pp. 291–294.

Critelli, S. (1999) The interplay of lithospheric flexure and thrust accommodation in forming stratigraphic sequences in the Southern Apennines foreland basin system, Italy. *Att. Accad. Naz. Lincei. Rendiconti Lincei. Sci. Fisiche Natur.*, **9**, 257–326.

Critelli, S., Arribas, J., Le Pera, E., Tortosa, A., Marsaglia, K.M. & Latter, K.K. (2003) The recycled orogenic sand provenance from an uplifted thrust belt, Betic Cordillera, southern Spain. *J. Sediment. Res.*, **73**, 72–81.

Curray, J.R. (1994) Sediment volume and mass beneath the Bay of Bengal. *Earth Planet. Sci. Lett.*, **125**, 371–383.

Damanti, J.F. (1993) Geomorphic and structural controls on facies patterns and sediment composition in a modern foreland basin. In: *Alluvial Sedimentation* (Ed. by M. Marzo & C. Puigdefabregas), *Int. Assoc. Sediment. Spec. Publ.* **17**, 221–233.

DeCelles, P.G. & Cavazza, W. (1999) A comparison of fluvial megafans in the Cordilleran (Upper Cretaceous) and modern Himalayan foreland basin systems. *Geol. Soc. Am. Bull.*, **111**, 1315–1334.

DeCelles, P.G. & DeCelles, P.C. (2001) Rates of shortening, propagation, underthrusting, and flexural wave migration in continental orogenic systems. *Geology*, **29**, 135–138.

DeCelles, P.G. & Giles, K.A. (1996) Foreland basin systems. *Basin Res.*, **8**, 105–123.

DeCelles, P.G. & Horton, B.K. (2003) Early to middle Tertiary foreland basin development and the history of Andean crustal shortening in Bolivia. *Geol. Soc. Am. Bull.*, **115**, 58–77.

de Sitter, L.U. (1952) Pliocene uplift of Tertiary mountain chains. *Am. J. Sci.*, **250**, 297–307.

Devlin, W.J., Rudolph, K.W., Shaw, C.A. & Ehman, K.D. (1993) The effect of tectonic and eustatic cycles on accommodation and sequence-stratigraphic framework in the Upper Cretaceous foreland basin of southwestern Wyoming. In: *Sequence Stratigraphy and Facies Associations* (Ed. by H.W. Posamentier, C.P. Summerhayes, B.U. Haq & G.P. Allen), *Int. Assoc. Sediment. Spec. Publ.* **18**, 501–520.

Dickinson, W.R. (1974) Plate tectonics and sedimentation. In: *Tectonics and Sedimentation* (Ed. by W.R. Dickinson), *SEPM Spec. Publ.* **22**, 1–27.

Dunn, J.F., Hartshorn, K.G. & Hartshorn, P.W. (1995) Structural styles and hydrocarbon potential of the sub-Andean thrust belt of southern Bolivia. In: *Petroleum Basins of South America* (Ed. by A.J. Tankard, R. Suarez & H.J. Welsink), *Am. Assoc. Petrol. Geol. Mem.*, **62**, 523–543.

Echavarria, L., Hernandez, R., Allmendinger, R. & Reynolds, J. (2003) Subandean thrust and fold belt of northwestern Argentina; geometry and timing of the Andean evolution. *Am. Assoc. Petrol. Geol. Bull.*, **87**, 965–985.

Ege, H., Sobel, E.R., Scheuber, E. & Jacobshagen, V. (2007) Exhumation history of the southern Altiplano plateau (southern Bolivia) constrained by apatite fission-track thermochronology. *Tectonics*, **26**, doi: 10.1029/2005TC001869.

Einsele, G., Ratschbacher, L. & Wetzel, A. (1996) The Himalaya-Bengal Fan denudation–accumulation system during the past 20 Ma. *J. Geol.*, **104**, 163–184.

Elger, K., Oncken, O. & Glodny, J. (2005) Plateau-style accumulation of deformation: Southern Altiplano. *Tectonics*, **24**, doi: 10/1029/2004TC001675.

Epis, R.C. & Chapin, C.E. (1975) Geomorphic and tectonic implications of the post-Laramide, late Eocene erosion surface in the southern Rocky Mountains. In: *Cenozoic History of the Southern Rocky Mountains* (Ed. by B.F. Curtis), *Geol. Soc. Am. Mem.*, **144**, 45–74.

Flemings, P.B. & Jordan, T.E. (1989) A synthetic stratigraphic model of foreland basin development. *J. Geophys. Res.*, **94**, 3851–3866.

Fuller, C.W., Willett, S.D., Hovius, N. & Slingerland, R. (2003) Erosion rates for Taiwan mountain basins: new determinations from suspended sediment records and a stochastic model of their temporal variation. *J. Geol.*, **111**, 71–87.

Geslin, J.K., Demko, T.M., Drzewiecki, P.A., Feldman, H.R., Hasiotis, S.T., McCrimmon, G.G., Van Wagoner, J.C. & Wellner, R.W. (2001). Sediment flux, paleoclimate, and sequence stratigraphy; lessons learned from numerical modeling. 7th International Conference on Fluvial sedimentology Proceedings, Open-File Report, University of Nebraska-Lincoln, Conservation and Survey Division, Report: OFR-60, 106.

Geslin, J.K., Demko, T.M., Drzewiecki, P.A., Feldman, H.R., Hasiotis, S.T., McCrimmon, G.G., Van Wagoner, J.C. & Wellner, R.W. (2002). Relative role of stream discharge, sediment flux, and baselevel change in stratal architecture of continental and nearshore sequences; results from forward numerical modeling. AAPG Annual Meeting Expanded Abstracts, 63.

Gohain, K. & Parkash, B. (1990) Morphology of the Kosi Megafan. In: *Alluvial Fans: A Field Approach* (Ed. by A.H. Rachocki & M. Church), pp. 151–178. John Wiley & Sons, Chichester, UK.

Gubbels, T.L. (1993) Tectonics and geomorphology of the eastern flank of the central Andes, 18–23°S latitude. Doctoral Thesis, Cornell University, Ithaca.

Gubbels, T.L., Isacks, B.L. & Farrar, E. (1993) High-level surfaces, plateau uplift, and foreland development, Bolivian central Andes. *Geology*, **21**, 695–698.

Gupta, S. (1997) Himalayan drainage patterns and the origin of fluvial megafans in the Ganges foreland basin. *Geology*, **25**, 11–14.

Hay, W.W., Wold, C.N. & Herzog, J.M. (1992) Preliminary mass-balanced 3-D reconstructions of the Alps and surrounding areas during the Miocene. In: *Computer Graphics in Geology* (Ed. by R. Pflug & J.W. Harbaugh), *Lect. Notes Earth Sci.*, **41**, 99–110.

Horton, B.K. (1999) Erosional control on the geometry and kinematics of thrust belt development in the central Andes. *Tectonics*, **18**, 1292–1304.

Horton, B.K. & DeCelles, P.G. (1997) The modern foreland basin system adjacent to the Central Andes. *Geology*, **25**, 895–898.

Horton, B.K. & DeCelles, P.G. (2001) Modern and ancient fluvial megafans in the foreland basin system of the Central Andes, southern Bolivia; implications for drainage network evolution in fold-thrust belts. *Basin Res.*, **13**, 43–63.

Hovius, N. & Leeder, M. (1998) Clastic sediment supply to basins. *Basin Res.*, **10**, 1–5.

Hulka, C. (2005) Sedimentary and tectonic evolution of the Cenozoic Chaco foreland basin, southern Bolivia. Doctoral Thesis, Freie Universitat, Berlin.

Hulka, C., Grafe, K.-U., Sames, B., Uba, C.E. & Heubeck, C. (2006) Depositional setting of the Middle to Late Miocene Yecua Formation of the Chaco Foreland Basin, southern Bolivia. *J. South Am. Earth Sci.*, **21**, 135–150.

Iriondo, M. (1993) Geomorphology and late Quaternary of the Chaco (South America). *Geomorphology*, **7**, 289–303.

Iriondo, M.H. (1984) The quaternary of northeastern Argentina. In: *Quaternary of South America and Antarctic Peninsula* (Ed. by J. Rabassa). **2**, 51–78.

Isacks, B.L. (1988) Uplift of the Central Andean Plateau and bending of the Bolivian Orocline. *J. Geophys. Res.*, **93**, 3211–3231.

Jordan, T.E. (1995) Retroarc foreland and related basins. In: *Tectonics of Sedimentary Basins* (Ed. by C.J. Busby & R.V. Ingersoll), pp. 331–362. Blackwell Science, Oxford.

Jordan, T.E. & Alonso, R.N. (1987) Cenozoic stratigraphy and basin tectonics of the Andes Mountains, 20°–28° south latitude. *Am. Assoc. Petrol. Geol. Bull.*, **71**, 49–64.

Jordan, T.E., Reynolds, J.H. III & Erikson, J.P. (1997) Variability in age of initial shortening and uplift in the Central Andes. In: *Tectonic Uplift and Climate Change* (Ed. by W.F. Ruddiman), pp. 41–61. Plenum Press, New York, NY.

Kennan, L. (2000) Large-scale geomorphology of the Andes; interrelationships of tectonics, magmatism and climate. Ed. by M.A. Summerfield), pp. 167–199. John Wiley & Sons, Chichester, UK.

Kennan, L., Lamb, S. & Rundle, J. (1995) K-Ar dates from the Altiplano and Cordillera Oriental of Bolivia; implications for Cenozoic stratigraphy and tectonics. *J. South Am. Earth Sci.*, **8**, 163–186.

Kennan, L., Lamb, S.H. & Hoke, L. (1997) High-altitude palaeosurfaces in the Bolivian Andes; evidence for late Cenozoic surface uplift. In: *Palaeosurfaces; Recognition, Reconstruction and Palaeoenvironmental Interpretation* (Ed. by M. Widdowson), *Spec. Publ. Geol. Soc. Lond.*, **120**, 307–323.

Kley, J. (1996) Transition from basement-involved to thin-skinned thrusting in the Cordillera Oriental of southern Bolivia. *Tectonics*, **15**, 763–775.

Kley, J. (1999) Geologic and geometric constraints on a kinematic model of the Bolivian Orocline. *J. South Am. Earth Sci.*, **12**, 221–235.

Kuhlemann, J., Frisch, W., Dunkl, I. & Szekely, B. (2001) Quantifying tectonic versus erosive denudation by the sediment budget; the Miocene core complexes of the Alps. *Tectonophysics*, **330**, 1–23.

Kuhlemann, J., Frisch, W., Szekely, B., Dunkl, I. & Kazmer, M. (2002) Post-collisional sediment budget history of the Alps; tectonic versus climatic control. *Int. J. Earth Sci.*, **91**, 818–837.

Lander, R.H. & Walderhaug, O. (1999) Predicting porosity through simulating sandstone compaction and quartz cementation. *Am. Assoc. Petrol. Geol. Bull.*, **83**, 433–449.

Latrubesse, E.M., Stevaux, J.C. & Singha, R. (2005) Tropical rivers. *Geomorphology*, **70**, 187–206.

Le Pichon, X., Fournier, M. & Jolivet, L. (1992) Kinematics, topography, shortening, and extrusion in the India–Eurasia collision. *Tectonics*, **11**, 1085–1098.

Leeder, M., Harris, T. & Kirkby, M. (1998) Sediment supply and climate change; implications for basin stratigraphy. *Basin Res.*, **10**, 7–18.

Leier, A.L., DeCelles, P.G. & Pelletier, J.D. (2005) Mountains, monsoons, and megafans. *Geology*, **33**, 289–292.

Marshall, L.G., Sempere, T. & Gayet, M. (1993) The Petaca (late Oligocene-middle Miocene) and Yecua (late Miocene) formations of the Subandean-Chaco Basin, Bolivia, and their tectonic significance. In: *Documents des Laboratoires de Geologie, Lyon*, **125** (Ed. by M. Gayet), 291–301. Departement des Sciences de la Terre, Universite Claude Bernard.

McMillan, M.E., Heller, P.L. & Wing, S.L. (20060) History and causes of post-Laramide relief in the Rocky Mountain orogenic plateau. *Geol. Soc. Am. Bull.*, **118**, 393–405.

McQuarrie, N. (2002) The kinematic history of the central Andean fold-thrust belt, Bolivia; implications for building a high plateau. *Geol. Soc. Am. Bull.*, **114**, 950–963.

McQuarrie, N., Barnes, J.B. & Ehlers, T.A. (2008) Geometric, kinematic, and erosional history of the central Andean Plateau, Bolivia (15–17°S). *Tectonics*, TC3007, doi: 10.1029/2006TC002054.

McQuarrie, N., Horton, B.K., Zandt, G., Beck, S. & DeCelles, P.G. (2005) Lithospheric evolution of the Andean fold-thrust belt, Bolivia, and the origin of the central Andean plateau. *Tectonophysics*, **399**, 15–37.

Moretti, I., Baby, P., Mendez, E. & Zubieta, D. (1996) Hydrocarbon generation in relation to thrusting in the Sub Andean Zone from 18 to 22°S, Bolivia. *Petrol. Geosci.*, **2**, 17–28.

Müller, J.P., Kley, J. & Jacobshagen, V. (2002) Structure and Cenozoic kinematics of the Eastern Cordillera, southern Bolivia (21°S). *Tectonics*, **21**, doi: 10.1029/2001TC001340.

Overeem, I., Syvitski, J.P.M., Hutton, E.W.H. & Kettner, A.J. (2005) Stratigraphic variability due to uncertainty in model boundary conditions; a case study of the New Jersey shelf over the last 40,000 years. *Mar. Geol.*, **224**, 23–41.

Patterson, P.E., Sprague, A.R., Hill, R.E. & McDonald, K.M.Anonymous (1995). Sequence stratigraphy and fluvial facies architecture, Farrer and Tuscher formations (Campanian), Tusher Canyon, UT. AAPG and SEPM Annual Meeting Abstracts 4, 74.

Pazzaglia, F.J. & Brandon, M.T. (1996) Macrogeomorphic evolution of the post-Triassic Appalachian Mountains determined by deconvolution of the offshore based sedimentary record. *Basin Res.*, **8**, 255–278.

Perez, R., Ghosh, S., Chatellier, J.-Y. & Lander, R.Anonymous (1999). Application of sandstone diagenetic modeling to reservoir quality assesment of the Misoa Formation, Bachaquero Field, Maracaibo Basin, Venezuela. AAPG Annual Meeting Expanded Abstracts, A107.

Phillips, J.D. & Gomez, B. (2007) Controls on sediment export from the Waipaoa River basin, New Zealand. *Basin Res.*, **19**, 241–252.

Placzek, C., Quade, J. & Patchett, P.J. (2006) Geochronology and stratigraphy of late Pleistocene lake cycles on the southern Bolivian Altiplano; implications for causes of tropical climate change. *Geol. Soc. Am. Bull.*, **118**, 515–532.

Robin, C., Rouby, D., Granjeon, D., Guillocheau, F., Allemand, P. & Raillard, S. (2005) Expression and modelling of stratigraphic sequence distortion. *Sediment. Geol.*, **178**, 159–186.

Robinson, R.A.J. & Slingerland, R.L. (1998a) Grain-size trends, basin subsidence and sediment supply in the Campanian Castlegate Sandstone and equivalent conglomerates of central Utah. *Basin Res.*, **10**, 109–127.

Robinson, R.A.J. & Slingerland, R.L. (1998b) Origin of fluvial grain-size trends in a foreland basin; the Pocono Formation on the central Appalachian Basin. *J. Sediment. Res.*, **68**, 473–486.

Roeder, D. & Chamberlain, R.L. (1995) Structural geology of sub-Andean fold and thrust belt in northwestern Bolivia. In: *Petroleum Basins of South America* (Ed. by A.J. Tankard, R. Suarez & H.J. Welsink), *Am. Assoc. Petrol. Geol. Mem.*, **62**, 459–479.

Schlunegger, F., Jordan, T.E. & Klaper, E.M. (1997) Controls of erosional denudation in the orogen on foreland basin evolution; the Oligocene central Swiss Molasse Basin as an example. *Tectonics*, **16**, 823–840.

Schlunegger, F., Melzer, J. & Tucker, G.E. (2001) Climate, exposed source-rock lithologies, crustal uplift and surface erosion; a theoretical analysis calibrated with data from the Alps/North Alpine foreland basin system. *Int. J. Earth Sci.*, **90**, 484–499.

Scott, G.R. (1975) Cenozoic surfaces and deposits in the southern Rocky Mountains. In: *Cenozoic History of the Southern Rocky Mountains* (Ed. by B.F. Curtis), *Geol. Soc. Am. Mem.*, **144**, 227–248.

Servant, M., Sempere, T., Argollo, J., Bernat, M., Feraud, G. & Lo Bello, P. (1989) Cenozoic morphogenesis and uplift of the Eastern Cordillera in the Bolivian Andes. *Comp. Rend. Acad. Sci. Paris*, **309**, 416–422.

Simpson, G. (2004) Dynamic interactions between erosion, deposition, and three-dimensional deformation in compressional fold belt setting. *J. Geophys. Res.*, **109**, doi: 10.1029/2003JF000111.

Simpson, G. (2006) Modelling interactions between fold-thrust belt deformation, foreland flexure and surface mass transport. *Basin Res.*, **18**, 125–143.

Sobel, E.R. & Strecker, M.R. (2003) Uplift, exhumation and precipitation: tectonic and climatic control of Late Cenozoic landscape evolution in the northern Sierras Pampeanas, Argentina. *Basin Res.*, **15**, 431–451.

Stock, G.M., Ehlers, T.A. & Farley, K.A. (2006) Where does sediment come from? Quantifying catchment erosion with detrital apatite (U-Th)/He thermochronometry. *Geology*, **34**, 725–728.

Tucker, G.E. & Slingerland, R.L. (1996) Predicting sediment flux from fold and thrust belts. *Basin Res.*, **8**, 329–349.

Uba, C.E., Heubeck, C. & Hulka, C. (2005) Facies analysis and basin architecture of the Neogene Subandean synorogenic wedge, southern Bolivia. *Sediment. Geol.*, **180**, 91–123.

Uba, C.E., Heubeck, C. & Hulka, C. (2006) Evolution of the late Cenozoic Chaco foreland basin, southern Bolivia. *Basin Res.*, **18**, 145–170.

Uba, C.E., Strecker, M.R. & Schmitt, A.K. (2007) Increased sediment accumulation rates and climatic forcing in the central Andes during the late Miocene. *Geology*, **35**, 979–982.

Van Wagoner, J.C. (1995) Sequence stratigraphy and marine to nonmarine facies architecture of foreland basin strata, Book Cliffs, Utah, U.S.A.. In: *Sequence Stratigraphy of Foreland Basin Deposits; Outcrop and Subsurface Examples from the Cretaceous of North America* (Ed. by J.C. Van Wagoner & G.T. Bertram), *Am. Assoc. Petrol. Geol. Mem.*, **64**, 137–223.

Van Wagoner, J.C., Beaubouef, R.T., Hoyal, D.C.J.D., Dunn, P.A., Adair, N.L., Abreu, V.L.D., Wellner, R.W., Awwiller, D.N., Sun, T., Deffenbaugh, M. & HUH, C. (2003). Energy dissipation and the fundamental shape of siliciclastic sedimentary bodies. AAPG and SEPM Annual Meeting Extended Abstracts, 175.

Widdowson, M. (1997) The geomorphological and geological importance of palaeosurfaces. In: *Palaeosurfaces: Recognition, Reconstruction and Palaeoenvironmental Interpretation* (Ed. by M. Widdowson), *Spec. Publ. Geol. Soc. Lond.*, **120**, 1–12.

Wilkinson, M.J., Marshall, L.G. & Lundberg, J.G. (2006) River behavior on megafans and potential influences on diversification and distribution of aquatic organisms. *J. South Am. Earth Sci.*, **21**, 151–172.

Manuscript received 10 September 2007; manuscript accepted 28 April 2008